

## ABSTRACT

Title of Document: Microfluidic Production of Polymeric Functional Microparticles  
Kunqiang Jiang, Doctor of Philosophy, 2013

Directed By: Professor Srinivasa R. Raghavan & Professor Don L. DeVoe

This dissertation focuses on applying droplet-based microfluidics to fabricate new classes of polymeric microparticles with customized properties for various applications. The integration of microfluidic techniques with microparticle engineering allows for unprecedented control over particle size, shape, and functional properties. Specifically, three types of microparticles are discussed here: (1) Magnetic and fluorescent chitosan hydrogel microparticles and their *in-situ* assembly into higher-order microstructures; (2) Polydimethylsiloxane (PDMS) microbeads with phosphorescent properties for oxygen sensing; (3) Macroporous microparticles as biological immunosensors.

First, we describe a microfluidic approach to generate monodisperse chitosan hydrogel microparticles that can be further connected *in-situ* into higher-order microstructures. Microparticles of the biopolymer chitosan are created continuously by contacting an aqueous solution of chitosan at a microfluidic T-junction with a stream of hexadecane containing a nonionic detergent, followed by downstream crosslinking of the generated droplets by a ternary flow of glutaraldehyde. Functional properties of the microparticles can be easily varied by introducing payloads such as magnetic nanoparticles and/or fluorescent dyes into the chitosan solution. We then use these

prepared microparticles as “*building blocks*” and assemble them into high ordered microstructures, i.e. microchains with controlled geometry and flexibility.

Next, we describe a new approach to produce monodisperse microbeads of PDMS using microfluidics. Using a flow-focusing configuration, a PDMS precursor solution is dispersed into microdroplets within an aqueous continuous phase. These droplets are collected and thermally cured off-chip into soft, solid microbeads. In addition, our technique allows for direct integration of payloads, such as an oxygen-sensitive porphyrin dye, into the PDMS microbeads. We then show that the resulting dye-bearing beads can function as non-invasive and real-time oxygen micro-sensors.

Finally, we report a co-flow microfluidic method to prepare uniform polymer microparticles with macroporous texture, and investigate their application as discrete immunological biosensors for the detection of biological species. The matrix of such microparticles is based on macroporous polymethacrylate polymers configured with tailored pores ranging from hundreds of nanometers to a few microns. Subsequently, we immobilize bioactive antibodies on the particle surface, and demonstrate the immunological performance of these functionalized porous microbeads over a range of antigen concentrations.

MICROFLUIDIC PRODUCTION OF POLYMERIC FUNCTIONAL  
MICROPARTICLES

By

Kunqiang Jiang

Dissertation to the Faculty of the Graduate School of the  
University of Maryland, College Park, in partial fulfillment  
of the requirements for the degree of  
Doctor of Philosophy  
2013

Advisory Committee:  
Professor Srinivasa Raghavan, Chair  
Professor Don DeVoe, Co-Chair  
Professor Michael Zachariah  
Professor Daniel Falvey  
Professor Philip Deshong  
Professor Gregory Payne

© Copyright by  
Kunqiang Jiang  
2013

## Dedication

This dissertation is dedicated to my parents and my family for all their love, supports and sacrifices over the years. They give me the courage to be here today.

## Acknowledgements

My four years of graduate study at Maryland have been always filled with learning, inspiration, and enjoyments. First I would like to thank my academic advisors, Professor Srinivasa Raghavan and Professor Don DeVoe, for providing the unique and wonderful opportunity to work in their groups and for their continuous guidance and encouragement over the years. I sincerely appreciate the unmatched dedication and patience they offer to their students and I am so blessed to have been one of them. They teach me valuable lessons on the importance of curiosity, determination and preservation through the journey of scientific research.

I want to give my sincere gratitude to my PhD committee members: Prof. Michael Zachariah, Prof. Daniel Falvey, Prof. Philip Deshong, Prof. Gregory Payne, for their guidance and mentorship throughout my graduate study. I am so thankful to have such an enriching experience working with them. In addition, I would like to thank Prof, Ian White for these insightful and fruitful discussions about ideas and projects.

I owe a lot of thanks to all of my peer colleagues in the labs of *Complex Fluids and Nanomaterials Group* and *Maryland MEMS & Microfluidics Lab*, for providing such a diverse, wonderful and always fun working environment. It has been a great pleasure to share thoughts with them and learn from them.

Special thanks go to all my friends at Maryland for these foods, movies, sports, as well as friendship and supports. I am grateful to have met each one of you.

To my parents and my family members, you are the people I owe the most. Thanks for all your love and encouragements that keep me brave and warm even I ran off thousands of miles away.

# Table of Contents

Dedication.....	ii
Acknowledgements .....	iii
Table of Contents .....	iv
List of Tables .....	vi
List of Figures .....	vii
Chapter 1. Introduction and Overview .....	1
1.1. Problem Description and Motivation .....	1
1.2. Proposed Approach.....	2
1.2.1. Hydrogel Microparticle and Their Assembly .....	2
1.2.2. Polydimethylsiloxane (PDMS) Microparticles .....	3
1.2.3. Macroporous Microparticles.....	4
1.3. Significance of This Work.....	5
Chapter 2. Background .....	7
2.1. The Science of Microparticles.....	7
2.2. Parameters to Characterize Microparticles.....	9
2.2.1. Composition.....	9
2.2.2. Particle Size and Particle Size Distribution.....	10
2.2.3. Geometric Shape .....	10
2.2.4. Functional Properties.....	11
2.3. Microfluidic Production of Microparticles.....	11
2.3.1. T-Junction.....	13
2.3.2. Flow-Focusing .....	14
2.3.3. Co-Flow.....	14
2.4. Factors that Control Droplet Generation.....	15
2.4.1. Capillary Number.....	15
2.4.2. Flow Rate Ratios.....	16
2.4.3. Liquid Viscosities.....	16
2.4.4. Sidewall Wettability.....	17
2.4.5. Effects of Surfactants.....	17
2.5. Polymerization of Droplet Precursors.....	18
2.5.1. Thermal Curing.....	18
2.5.2. UV Crosslinking.....	19
2.5.3. Chemical Crosslinking.....	20
2.6. Fabrication of Microfluidic Devices.....	21
2.6.1. PDMS Soft Lithography.....	21
2.6.2. Thermoplastic Microfabrication.....	22
2.6.3. Capillary Assembly.....	23

Chapter 3. Microfluidic Production and Assembly of Chitosan Microparticles.....	25
3.1. Introduction .....	25
3.2. Experimental Section.....	29
3.3. Results and Discussion.....	31
3.3.1. Droplet Generation and Conversion to Robust Microparticles.....	31
3.3.2. Linking Microparticles into Microchains.....	34
3.3.3. Magnetic Chains of Varying Flexibility.....	37
3.3.4. Future Outlook.....	40
3.4. Conclusions.....	41
Chapter 4. Monodisperse PDMS Microbeads as Discrete Oxygen Sensors.....	42
4.1. Introduction.....	42
4.2. Experimental Section.....	45
4.3. Results and Discussion.....	47
4.3.1. Microfluidic Production of PDMS Microparticles.....	47
4.3.2. Performance as Oxygen Sensors.....	51
4.4. Conclusions.....	52
Chapter 5. Microfluidic Synthesis of Macroporous Polymer Immunobeads.....	54
5.1. Introduction.....	54
5.2. Experimental Section.....	57
5.3. Results and Discussion.....	59
5.3.1. Macroporous Microsphere Synthesis.....	59
5.3.2. Immunobead Functionalization.....	66
5.3.3. Immunobead Performance.....	70
5.4. Conclusions.....	74
Chapter 6. Conclusions and Recommendations.....	76
6.1. Project Summary and Principal Contributions.....	76
6.2. Recommendations for Future Work.....	78
6.2.1. Chitosan Microparticle Assembly.....	78
6.2.2. PDMS Microparticles: Synthesis and Other Applications.....	80
6.2.3. Macroporous Microparticles: Other Applications.....	82
References.....	83

## List of Tables

Table 2.1. Brief summary of important aspects in the production of microparticles.....	9
Table 2.2. General considerations for microfluidic production of microparticles.....	12
Table 6.1. Brief summary of polymeric functional microparticles developed in this thesis.....	76

## List of Figures

Figure 1.1. A new approach to “micro-manufacturing”: microfluidic fabrication of magnetic and fluorescent chains using chitosan microparticles as building blocks.....	2
Figure 1.2. Schematic illustration of the production process of PDMS microparticles on a flow focusing thermoplastic device. These produced PDMS microparticles can be further functionalized with various encapsulants.....	3
Figure 1.3. Uniform polymer microparticles with macroporous textures. The surface of these microparticles has been modified with bioactive species so that they can serve as high performance immunobeads.....	4
Figure 2.1. Dimensional scale for various types of natural and synthetic objects. The scope of microparticle research focuses on the size scale ranging from 500 nm to 500 $\mu\text{m}$ . Control over particle size, composition, geometry and functionality is the main focus in microparticle research.....	8
Figure 2.2. Schematic illustration of different types of droplet generators including T-Junction, Flow Focusing and Co-Flow configurations.....	13
Figure 2.3. Schematic illustration of typical fabrication procedures for microfluidic devices via PDMS soft lithography.....	21
Figure 2.4. Schematic illustration of the fabrication routes of thermoplastics microfluidic devices. Top route: hot embossing method; bottom route: direct micro-machining.....	23
Figure 2.5. Schematic illustration of procedures for droplet generator assembled from capillaries. (a) capillary pulling under heat; (b) breakage of the pulled tip via microforging; (c) assembled microdroplet generator; (d).microscopic image of such a device.....	24
Figure 3.1. Microfluidic generation of chitosan microparticles. The channels have a rectangular cross-section (125 $\mu\text{m}$ height and 100 $\mu\text{m}$ width). At the T-junction, the dispersed phase (an aqueous chitosan solution) is contacted with the continuous phase (a solution of the detergent, Span 80 in hexadecane), and in turn, discrete aqueous droplets are formed. These droplets travel down the channel and meet the flow of the incubation phase, which consists of glutaraldehyde (GA) emulsified in hexadecane using Span 80. The GA crosslinks the droplets as they travel through the long, serpentine channel segment. Ultimately, the droplets are converted into particles and these are collected in the reservoir at the end. The inset shows a single microparticle: note that the chitosan chains are covalently linked by GA and the particle is stabilized in hexadecane by detergent molecules. ....	28

Figure 3.2. Optical micrographs of: (a) spherical chitosan-bearing aqueous droplets in hexadecane (these were not contacted with GA); (b) plug-like microparticles formed by crosslinking the above droplets with GA; (c) the above microparticles transferred from hexadecane to deionized water, and (d) close-up of a single microparticle in water. Note that the droplets/particles contain MNPs, and the black spots in the images correspond to aggregates of these MNPs. ....33

Figure 3.3. (a) Schematic depiction of the on-chip process for linking individual particles into chains. (1) A stainless steel wire is used as a valve to block the channel outlet, (2) the wire is held until the desired number of subunits has been accumulated on the chain, and (3) the wire is then removed and the chain is flushed into the reservoir. (b) Optical micrograph showing a close-up of the assembled chain inside the microchannel. ....35

Figure 3.4. (a) Schematic of the modified chip design used to prepare chains of alternating particles. The chip has two T-junctions, corresponding to two dispersed phases. One dispersed phase has 0.1% of the fluorescent dye, sodium fluorescein while the other does not contain dye. When the flow rates of the two dispersed phases are set equal, an alternating sequence of drops with and without the dye travel down the channel, where they are fixed into chains as described in Figure 3.3. (b) Fluorescence micrograph showing a particle chain with alternating fluorescent and non-fluorescent subunits..... 36

Figure 3.5. Rotation of a rigid magnetic chain when a bar magnet is rotated above the holding container. The chain is formed by extensive fusion of three chitosan particles bearing MNPs and a fluorescent dye. (1) to (3) represent successive images taken using a fluorescence microscope. Arrows indicate the direction of the net (induced) magnetic dipole at each instant. .... 38

Figure 3.6. Undulating or “beating” motion of a semiflexible magnetic chain when a magnet is swayed on top of the holding container. (1) to (6) represent successive images obtained using a bright-field optical microscope. Scale bars in all images are 200  $\mu\text{m}$ ....39

Figure 4.1. Illustration of the scheme for producing PDMS microbeads that can be used as oxygen sensors. (a) Microfluidic generation of PDMS droplets bearing a phosphorescent dye by flow-focusing on a PMMA microfluidic device; (b) Off-chip curing of the PDMS droplets at 70°C; (c) Rinsing and harvest of the resulting dye-bearing microbeads; (d) Use of these microbeads for oxygen sensing. ....43

Figure 4.2. (a) Formation of PDMS-bearing droplets by flow focusing. The PDMS precursor stream is the central flow through the channel, while the side streams are both aqueous solutions of 5 wt% SDS. (b) Uncured PDMS droplets remain stable in a glass vial without coalescence or aggregation.....48

Figure 4.3. Images of cured PDMS microbeads from: (a) optical microscopy; and (c) SEM. In (b) the size distribution of microbeads in (a) is plotted. The average diameter of

the beads is 80  $\mu\text{m}$  with a standard deviation of 1.8  $\mu\text{m}$ . A Gaussian fit to the distribution is also shown. .... 49

Figure 4.4. (a) Optical microscope images showing contrast in phosphorescence intensity of a PtTFPP-bearing PDMS microbead (150  $\mu\text{m}$  diameter) at various oxygen levels. (b) Plot of phosphorescence intensity vs. oxygen partial pressure. The phosphorescence is significantly quenched with increasing oxygen levels, and the response follows the Stern-Volmer equation (eq 4.1), as shown by the inset plot. Data points indicate the mean values from eight beads with standard deviations given by the vertical error bars. .... 50

Figure 5.1. Schematic of the macroporous microsphere synthesis and surface modification process: (I) Microfluidic generation of droplet precursors in a co-flow droplet generator, with the dispersed phase composed of monomer GMA, crosslinker SR454, porogen DA, and photoinitiator DMPA sheared into discrete droplets by a continuous phase comprising an aqueous solution with surfactants. (II) UV photopolymerization of the droplet precursors for the formation of stable macroporous microspheres; (III) Immobilization of capture antibody on the pore surfaces converts the microspheres into active immunobeads. (IV) Direct immunoassay test of immunobeads using fluorescent labeled antigen. .... 56

Figure 5.2. (a) Optical micrograph of monodisperse macroporous microspheres prepared from the precursor recipe with monomer GMA, crosslinker SR454 and porogen DA. (b) Electron micrograph of a single microbead revealing its macroporous structure. (c) Magnified view of the porous morphology. (d) Optical microscope image of solid non-porous microbeads without the addition of porogen DA during preparation. (e) Electron micrograph of a non-porous microbead. (f) Magnified view of a solid bead surface revealing the lack of macroporosity. .... 61

Figure 5.3. (a) SEM image of a cleaved macroporous microspheres revealing uniform porosity throughout the particle volume. (b) Size distributions of both macroporous microspheres and solid non-porous microparticles showing excellent size uniformity. Data was obtained with a sample size of 100 microbeads in each case. .... 64

Figure 5.4. (a)&(b) Schematic illustrations of the GMBS and glutaraldehyde routes for immobilization of antibody on the monolith surface. (c) Auto-fluorescence measurements after each modification step reveals that the GMBS route reduces background fluorescence compared to the glutaraldehyde route by over 2 logs. .... 67

Figure 5.5. Performance of anti-IgG functionalized immunobeads at different FITC-IgG concentrations. Control samples with deactivated anti-IgG on both macroporous microspheres and non-porous microbeads were also prepared to assess differences between specific and non-specific binding. Error bars reflect the standard deviation of fluorescence measurements performed from 10 individual immunobeads. .... 71

Figure 6.1. Bi-functional dimers assembled from chitosan microparticles, each lobe of the dimer can have distinctive properties. The assembly process is achieved in-situ by a highly controlled microfluidic-mediated coalescence behavior that pairs two individual droplets together automatically. .... 79

Figure 6.2. The significant swelling of PDMS microparticle in the oil-based limonene compound demonstrates their excellent loading capacity for hydrophobic encapsulants. It allows these PDMS microparticles to be used as controlled release carriers which can carry a load of encapsulants and then slowly release them..... 81

# Chapter 1

## INTRODUCTION AND OVERVIEW

### 1.1. PROBLEM DESCRIPTION AND MOTIVATION

Polymeric microparticles are used in many areas such as chromatography, targeted drug delivery, and medical and personal care products. A variety of conventional methods such as emulsion polymerization, spray drying, sol-gel processing and template-assisted generation have been used to prepare such microparticles. However, these methods still suffer from several problems, including large variations in size and properties from particle to particle, limited selection of available materials and methods, large consumption of chemicals and energy, as well as high costs of production. As a result, there is a growing need to develop simple and versatile techniques to produce microparticles with precise control over their size, geometry, and functional properties.

Recently, microfluidics has emerged as a promising option to overcome many of the limitations of conventional methods. In droplet microfluidics, reactants are dispersed very precisely into uniform individual microdroplets, and these droplets can be converted into solid microparticles by various means. As a result, microfluidics gives us the capabilities to precisely control the properties and functionalities of microparticles. For example, microparticles of outstanding size uniformity can be achieved with polydispersities of less than 5%. Also, various particle shapes (e.g. spheres, cylinders, plug shapes) can be fabricated in a highly controlled manner. Also, the continuous nature

of microfluidics ensures a reasonable throughput production of particle production, with generation rates up to thousands of particles per second.

## 1.2. PROPOSED APPROACH

In this dissertation, we are interested in using droplet microfluidics to produce new classes of polymeric microparticles with advanced functional properties. We will describe the synthesis of three different classes of microparticles and in each case, the microfluidic synthesis of such particles is reported here for the first time.

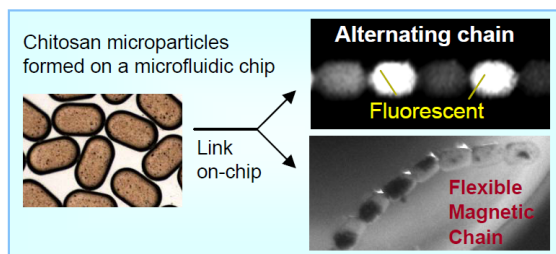


**Figure 1.1.** A new approach to “micro-manufacturing”: microfluidic fabrication of magnetic and fluorescent chains using chitosan microparticles as building blocks.

### 1.2.1. Hydrogel Microparticles and Their Assembly

First, in Chapter 3, we describe an approach to synthesize hydrogel microparticles and moreover to create higher-order structures of these particles *in situ* within a microfluidic device. The hydrogel microparticles are made of the biopolymer chitosan and are created on a microfluidic T-junction platform by dispersing an aqueous solution of chitosan into another stream of an immiscible oil phase. Monodisperse chitosan droplets (~ 150  $\mu\text{m}$  diameter) are continuously produced, and are crosslinked by a

downstream flow of glutaraldehyde. The functional properties of these microparticles are adjusted by introducing various payloads during the preparation stage, such as magnetic nanoparticles and/or fluorescent dyes. We then demonstrate the assembly of individual particles into covalently linked chains of precise length, using glutaraldehyde again as the chemical “glue”. The arrangement of microparticles within a chain can also be precisely controlled, e.g., to generate linear chains with alternating fluorescent and non-fluorescent subunits. Besides, the chain flexibility can be tuned by simply adjusting the crosslinking conditions. Overall, we suggest that microfluidic chips could serve as a micro-manufacturing platform in which the building blocks (microparticles) could be connected and positioned into structures of arbitrary arrangement and complexity.

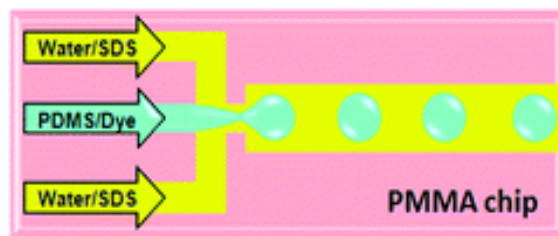


**Figure 1.2.** Schematic illustration of the production process of PDMS microparticles on a flow focusing thermoplastic device. These produced PDMS microparticles can be further functionalized with various encapsulants.

### 1.2.2. Polydimethylsiloxane (PDMS) Microparticles

Next in Chapter 4, we describe a microfluidic approach to generate monodisperse microparticles of the well-known elastomer, PDMS. We utilize a planar flow-focusing configuration for the dispersion of viscous PDMS precursor solutions into uniform microdroplets. Discrete PDMS droplets with narrow size distribution are produced and

are collected in a glass vial. Subsequent thermal curing turns these droplets into stable microparticles with diameters ranging from 50 to 200  $\mu\text{m}$ . These PDMS microparticles can have a variety of applications. For example, the high permeability of PDMS to oxygen molecules allows these beads to be used as oxygen sensors. To demonstrate this, we integrate an oxygen-sensitive phosphorescent dye into these PDMS microparticles, and we demonstrate that the resulting beads can function as quantitative, non-invasive sensors of oxygen concentrations in real-time.

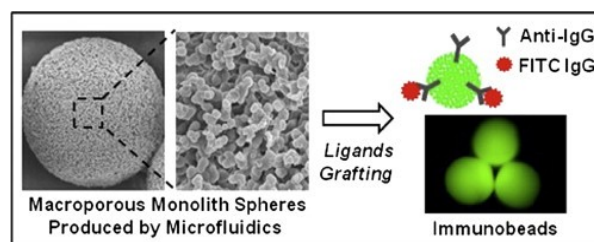


**Figure 1.3.** Uniform polymer microparticles with macroporous textures. The surface of these microparticles has been modified with bioactive species so that they can serve as high performance immunobeads.

### 1.2.3. Macroporous Microparticles

Finally, in Chapter 5, we present the preparation of a new type of immunosensors employing microfluidically prepared macroporous microparticles. The microparticles are produced using a simple microfluidic tubing co-flow droplet generator that gives rise to droplets containing methacrylate monomers and an alcohol as porogen. Upon polymerization and subsequent removal of the porogen, particles with exceptional size uniformity and controllable macroporosity are produced. Subsequent grafting treatments are utilized to anchor immunoactive ligands on the porous particle surfaces, converting these microparticles into discrete immunosensing elements. Then a direct immunoassay

is carried out to test the performance of these immunosensors, and the results show good detection limits and binding specificity.

### **1.3. SIGNIFICANCE OF THIS WORK**

Our studies provide a deeper understanding of droplet microfluidics and its use for the production of next-generation functional microparticles. From a scientific standpoint, we provide useful guidelines for the preparation of functional microparticles using microfluidics. Typical examples of microfluidic droplet generation methods, including T-junction, flow focusing and co-flow, have been represented in each of the three examples above. The commonly encountered emulsification mechanisms in droplet generation (i.e. water-in-oil emulsion and oil-in-water emulsion) have also been covered systematically in this study. Additionally, the compositions of these microparticles have been varied from soft hydrogel of natural biopolymers, elastomers of PDMS, and rigid plastics of methacrylate copolymers. Besides, we have explored a number of functionalization methods to engineer the properties of these prepared microparticles, including direct encapsulation of functional moieties as well as subsequent surface modification with additional functional species.

Regarding the application potential of the functional microparticles we have developed in this study, the chitosan hydrogel microparticles (and their chains) could find application in various fields like micro-fabrication, magnetic actuators and bio-mimics. As for the monodisperse PDMS microparticles, they possess many advantageous properties including being inert, biocompatible and transparent, and thus can be used in

personal care and healthcare applications. Finally, with regard to the macroporous methacrylate microparticles, the combination of their macroporous texture and bio-affinity enables them to be used either as individual biosensors, or as a stationary phase to be packed in chromatographic columns.

## Chapter 2

### BACKGROUND

This dissertation is concerned with the microfluidic production of functional microparticles. In this chapter, we begin with a brief introduction to microparticles and their properties. We then switch to the microfluidic techniques and discuss the process of droplet formation and the factors of importance there. Additionally, we review various polymerization methods that are developed to convert liquid droplets into stable microparticles. After that, typical fabrication routes of microfluidic devices are briefly summarized. The summary here is intended to provide the reader a general idea on the basic procedures involved in droplet microfluidics as well as on the recent progress that has been achieved in the field.

#### 2.1. THE SCIENCE OF MICROPARTICLES

Microparticles or microscale colloids are small objects covering a range of size between  $\sim 500$  nanometers to 500 micrometers (Figure 2.1).<sup>1</sup> Microparticles are of great scientific interest as they effectively connect the dimensional gap between bulk materials and the nano-sized atoms and molecules. Besides, microparticles exhibit some fascinating physicochemical properties that differ from those observed in their bulk counterparts. These properties include: unique optical and mechanical properties, enhanced specific surface area, high mobility and dispersion stability.<sup>1-4</sup>

New applications of microparticles are discovered every day in various application fields. For example, in biological research, magnetic microspheres of specific affinity are used to assay and isolate cells.<sup>5</sup> In analytical chemistry, silica microparticles are closely packed in chromatographic beds to improve the efficiency of sample preparation and separation.<sup>3</sup> In pharmaceutical applications, therapeutic agents like drugs are encapsulated in polymer microparticles in order to achieve controlled release over prolonged time.<sup>6</sup> Moreover, in many personal care and cosmetic products, microparticles are added to hide wrinkles and smooth skins.<sup>7</sup>

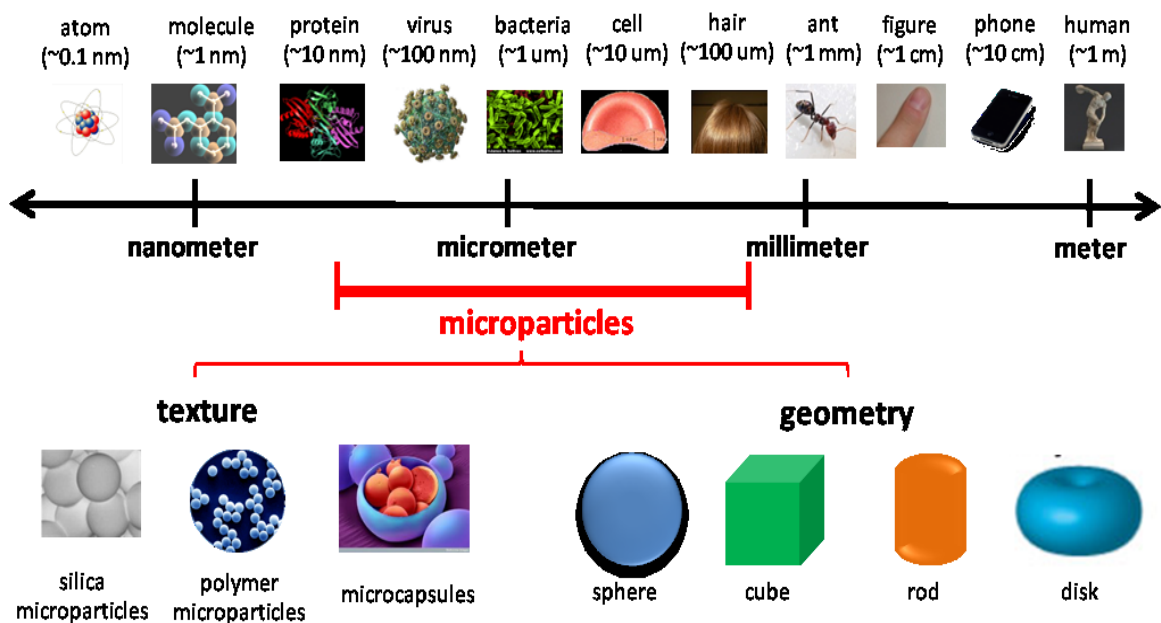


**Figure 2.1.** Dimensional scale for various types of natural and synthetic objects. The scope of microparticle research focuses on the size scale ranging from 500 nm to 500 μm. Control over particle size, composition, geometry and functionality is the main focus in microparticle research.

## 2. 2. PARAMETERS TO CHARACTERIZE MICROPARTICLES

When selecting microparticles for different applications, their composition, functional properties, and sizes must be carefully considered. Several key criteria that describe the physical and functional properties of microparticles are summarized in Table 2.1 and discussed below.

**Table 2.1.** Brief summary of important aspects in the production of microparticles

Microparticle “Engineering”			
Composition	Size	Geometry	Functionality
glass	uniform	sphere	magnetic
polymer		cube	fluorescent
metal	adjustable	rod/disk	chemical/bio specific
ceramics		capsule	degradable

### 2.2.1. Composition

Microparticles can be composed of many natural and synthetic materials, such as ceramics, silica, and polymers. Glass microparticles are popular because of their excellent mechanical, electrical, optical, thermal and chemical properties. For example, uniform glass microspheres are electrical insulators, and thus can be used as bond spacers in electronic components (such as flat panel displays) to provide precise positioning and spacing.<sup>8</sup> Polymeric materials have also been widely used to prepare microparticles. Recent interest has also been focused on stimuli responsive polymers, which can be engineered to be environmentally sensitive to external stimuli such as pH, temperature, or the concentration of chemicals. Microparticles made from such polymers can have the

capability to change their shapes/behaviors as result of a change in external stimuli; they are thus termed “smart” or “intelligent” microparticles.<sup>9</sup>

### 2.2.2. Particle Size and Particle Size Distribution

A key parameter to characterize microparticles is the particle size since many of their physical and chemical properties are size-dependent, including enhanced specific surface, suspension stability, particle mobility, and so on.<sup>1</sup> The particle size distribution is used to characterize the uniformity of microparticles in size. A narrow size distribution of the particles is often desirable. One way to quantify particle size distribution is in terms of the coefficient of variation ( $CV$ ), which is defined as:

$$CV = \left(\frac{\sigma}{\mu}\right) \times 100\% \quad (\text{eq 2.1})$$

where  $\sigma$  represents the standard deviation of particle diameters and  $\mu$  refers to the mean particle diameter. In many cases, size distributions are presented as histogram plots that show the percentage of particles found in each size range.

### 2.2.3. Geometric Shape

Microparticles can be engineered into various shapes. Most synthetic microparticles are spherical or nearly spherical because the spherical shape minimizes interfacial energy. However, microparticles with non-spherical or anisotropic shapes (such as cubes, rods, disks) are desirable in a variety of applications. For example, compared to spheres, it has been found that cylinder-shaped microparticles of high aspect ratios are advantageous for drug delivery since they can permeate more easily into biological cells.<sup>10</sup> Microparticles with rod-like or corkscrew-like morphologies can have

biomimetic transport properties because of the similarity of their shapes to those of viruses and bacteria.<sup>11</sup>

#### **2.2.4. Functional Properties**

For many applications, microparticles are engineered to have functional properties. For example, microparticles can be engineered to be magnetic so that they can be manipulated with the help of external magnetic fields. In imaging applications such as blood flow tracing, *in vivo* imaging and multiplexed flow cytometry, microparticles are engineered to be fluorescent to provide better visualization. For diagnostics and separation applications, the surface of microparticles are coated with affinity ligands (such as antibodies/antigens, peptides, nucleic acids, proteins like avidin/streptavidin, biotin, etc.), so that the particles could have the capability to capture or bind selectively to molecules in solution.<sup>12-13</sup>

### **2.3. MICROFLUIDIC PRODUCTION OF MICROPARTICLES**

Microparticles are often prepared via routes that involve emulsification. A precursor mixture is dispersed into droplets in a continuous, immiscible phase. Then these droplets are solidified into microparticles. In traditional emulsification methods, large quantities of droplets are produced in bulk containers under vigorous agitation/stirring. However, due to the crude agitation process, bulk methods offer little control over droplet generation. In turn, the resulting microparticles are generally not uniform in size.<sup>14</sup>

Droplet microfluidics is an alternative to improve the monodispersity of microparticles. Here, the process of emulsification (droplet generation) is conducted within geometrically confined microchannels and in turn, the process is highly controlled. The resulting microdroplets are of uniform size with coefficients of variance less than 5%.<sup>15</sup> After preparation, these droplets precursors can then be polymerized (crosslinked) to form stable solidified microparticles. In principle, nearly any polymeric precursor can be transformed into microparticles with the help of droplet microfluidics as long as a suitable emulsification method can be found and an appropriate polymerization method is available. Droplet polymerization can be categorized into *in-situ* polymerization and *off-chip* polymerization.<sup>16</sup> In the *in-situ* case, the polymerization occurs within the microfluidic device, while in the *off-chip* process, droplets are usually collected after the outlet of microfluidic device and then polymerized.

**Table 2.2.** General considerations for microfluidic production of microparticles

Device Fabrication	Generator Configuration	Emulsion Type	Polym. Location	Polym. Mechanism
Soft lithography	T-Junction	Oil in Water	in situ	Thermal Curing
Micro-machining	Flow Focusing	Water in Oil	off chip	Photo Polymerization
Capillary Assembly	Co Flow	Double emulsion		Chemical Crosslinkage

A variety of microfluidic droplet generators with different geometric configurations are available to produce droplets. Three of them are most frequently

applied: “T-junction”, “Flow Focusing”, and “Co-Flow”. These are illustrated schematically in Figure 2.2 and are discussed below.

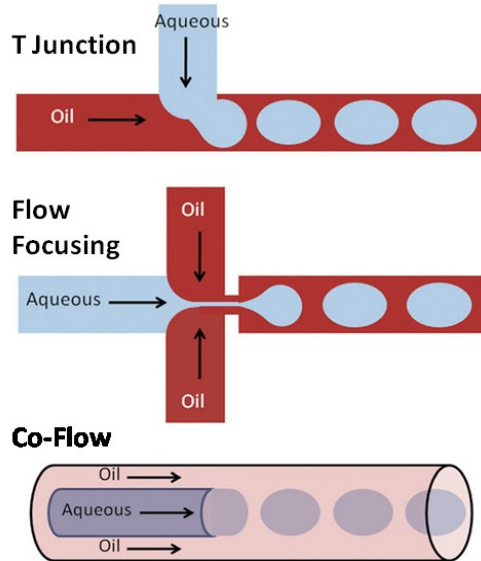


**Figure 2.2.** Schematic illustration of different types of droplet generators including T-Junction, Flow Focusing and Co-Flow configurations.<sup>17</sup>

### 2.3.1. T-Junction

T-junction was the first type of droplet generator used to produce monodisperse droplets inside a microfluidic channel, and it is still widely used today. In the T-junction configuration (Figure 2.2), the dispersed phase is injected perpendicularly into a main stream of the continuous phase. The break-up of the dispersed flow into discrete droplets is caused by the shear force exerted by the continuous phase at the T-junction interface. Besides its simplicity, one additional benefit of the T-junction is the possibility to align multiple generators in sequence and produce different types of droplets at synchronized

frequencies, which is of critical importance in applications such as droplet coalescence and droplet assembly.<sup>18-19</sup>

### **2.3.2. Flow-Focusing**

Another configuration for droplet generation is called “flow focusing”, in which the dispersed phase and continuous phase are focused to pass through a small orifice right after the two flows meet (Figure 2.2). Due to the geometric confinement in the orifice, the dispersed and continuous phases are squeezed into elongated, thinner flows with distinctive boundaries. Then the dispersed flow decays into discrete droplets. One advantage of “flow focusing” droplet generators is that they can produce droplets smaller than the dimension of the channel because of the “squeezing” effect of the two flows.<sup>15</sup> Flow-focusing also provides high frequencies of droplet generation, i.e., it allows for higher throughput.

### **2.3.3. Co-Flow**

The “co-flow” geometry is somewhat similar to “flow focusing” in its underlying principle, but the two differ in their geometric configurations.<sup>20-21</sup> In “co-flow”, the dispersed and continuous phases are introduced along axisymmetric, parallel microchannels (Figure 2.2). Unlike the 2-D planar “flow focusing” device, the “co-flow” configuration abbreviates the small orifice that confines the two flows. The dispersed phase is directly surrounded by the continuous phase 3-dimensionally without the squeezing process. One attractive feature of the “co-flow” configuration is that it can be created using commercially available capillaries and tubes (details in Section 2.6.3.).<sup>22</sup> In

other words, it can be implemented without the need for a microfluidic chip. One additional benefit of “co-flow” devices is that it minimizes contact of the dispersed phase with the side walls of microchannels and so it is less restrictive on the wetting properties at this interface.<sup>22</sup>

## 2.4. FACTORS THAT CONTROL DROPLET GENERATION

Besides the configuration of the droplet generators and the dimensions of the channels, the formation of droplets within a microfluidic device is controlled by a number of parameters including flow rate ratios, fluid viscosities, the presence of surfactants, as well as the wettability of channel sidewalls.

### 2.4.1. Capillary Number

The mechanism of droplet break-off relies on the competing interaction between the viscous shearing of the continuous phase and the interfacial tension of the two phases (Rayleigh-Plateau instability). The dimensionless capillary number  $Ca$  represents the relative effect of viscous shear forces versus surface tension on droplet formation:

$$Ca = \frac{\eta v}{\gamma} \quad (\text{eq 2.2})$$

where  $\eta$  (Pa.s) and  $v$  (m/s) are the viscosity and the velocity of the continuous phase, respectively.  $\gamma$  (N/m) refers to the interfacial tension between the two immiscible phases.<sup>15</sup> Droplet formation occurs when the capillary number is above a critical capillary number  $Ca^*$ , which characterizes a critical state at which the viscous shearing force is

strong enough to overcome the surface tension.  $Ca^*$  is dependent on the channel size and generator geometry.

#### **2.4.2. Flow Rate Ratio**

Different modes of droplet generation can be achieved by adjusting the ratio of the flow rates of the two immiscible flows. The flow rate ratio (FRR) is usually defined as the ratio of the dispersed phase to the continuous phase. The droplet size tends to decrease when a higher flow rate of the continuous phase is used (for a fixed flow rate of the dispersed phase). This is possibly due to the greater shearing force exerted on the dispersed phase when the continuous phase is moving rapidly.<sup>15</sup> On the other hand, increasing the dispersed phase flow rate allows the production of droplets at a higher frequency.

#### **2.4.3. Liquid Viscosities**

It is also important to consider the relative values of the viscosities of the dispersed and continuous phases for stable droplet formation. For example, it is easier to break the dispersed phase into droplets when a more viscous continuous phase is used, as a stronger shear force is provided. On the other hand, if the dispersed flow is viscous, it can be difficult to form droplets due to insufficient shearing. This can be a problem when viscous polymeric solutions of high molecular weight or high concentration are used as the dispersed phase.<sup>23</sup> Correspondingly, sometimes it is necessary to decrease the viscosity of the dispersed phase to help generate droplets, which can be done by either

diluting the dispersed phase with less viscous co-solvents, or by running the experiment at elevated temperature.

#### **2.4.4. Sidewall Wettability**

Stable droplet formation is also dependent on the wettability of channel sidewalls as the sidewalls need to be completely wetted by the continuous phase.<sup>16</sup> Specifically, hydrophobic channels are needed for water-in-oil droplet generation, and hydrophilic channels are necessary for the dispersion of oil droplets in aqueous solution. Inappropriate combination of surface wetting and emulsion type results in the unwanted adhesion of the dispersed phase on the channel sidewall, thus making it difficult for it to be sheared into droplets. Because of this, additional treatments are needed to tune the microchannel surface wettability for certain circumstances. Sometimes soaking the microchannels with surfactant-laden continuous phase works, as it imposes a coating of surfactants on the microchannel surfaces. For example, polymethyl methacrylate (PMMA) channels are slightly hydrophilic, but they can be made hydrophobic by the addition of nonionic surfactants such as SPAN 80 or TWEEN 20.<sup>24</sup>

#### **2.4.5. Effects of Surfactants**

Surfactants are needed to generate droplets in microfluidic systems for several reasons. First, surfactants coat the formed droplets, thus preventing undesired droplet coalescence and fusion. This improves the stability of droplets after they are formed. In addition, sometimes surfactants are added to alter the wetting property of microchannels, as mentioned above. Surfactants also reduce the interfacial energy barrier that needs to be

overcome during droplet formation. The energy barrier arises due to the higher interfacial area of the droplet compared to the fluid stream, and crossing the barrier is accomplished by the shear forces exerted by the continuous phase. In this context, surfactants reduce the energy penalty in forming the droplet and thus facilitate droplet generation.

## **2.5. POLYMERIZATION OF DROPLET PRECURSORS**

A variety of methods have been developed to polymerize or crosslink droplets into solid microparticles. They can be broadly classified into three categories with regard to the mechanisms involved: 1) Thermal Curing, 2) UV Crosslinking, and 3) Chemical Crosslinking.

### **2.5.1. Thermal Curing**

Thermal curing utilizes thermal-initiated polymerization to crosslink droplets containing monomers, thermo-initiators, and solvents. This method has been demonstrated successfully to prepare a number of useful microparticles of thermoplastics, including polystyrene (PS),<sup>25</sup> polydivinylbenzene (PDVB)<sup>26</sup> and poly(isobornyl acrylate) (PIBA)<sup>27</sup>. It has also been applied to prepare PDMS microbeads by thermal condensation polymerization of PDMS precursors.<sup>28</sup> The “*off-chip*” approach is usually used in the case of thermal curing because it typically requires more time than the typical retention time of droplets within the microchannel. In addition, “*off-chip*” methods provide better temperature control and thus allow better control of the kinetics of thermal curing.

Another method of thermal curing involves cooling droplets from an elevated temperature to a temperature below the melting or gel point of the material. Hydrogel microparticles composed of biopolymer gelatin have been prepared through this method, in which a 40 °C gelatin flow was first emulsified into droplets, which were collected in a *off-chip* container at 25 °C.<sup>29</sup> Additional cooling of these droplets at a temperature of 5 °C induces the physical crosslinking of gelatin molecules, solidifying them into particles. In addition, microparticles of alloy metals (fusible at relative low temperatures, ~ 50 °C) have also been prepared using similar approaches.<sup>30</sup>

### **2.5.2. UV Crosslinking**

Microparticles can also be crosslinked by ultraviolet (UV) polymerization, which involves crosslinking of droplets containing monomers, UV-initiators, and solvents upon exposure to external UV radiation. The UV-initiated free radical polymerization of acrylate moieties is a typical example. The success of UV polymerization depends on several factors. For example, the material of the microfluidic device must be transparent to UV wavelengths for “*in-situ*” crosslinking. Also, sometimes it is important to remove oxygen and other inhibitors from the precursor solutions (e.g., by purging nitrogen).

One advantage of UV polymerization is its ability to be integrated with photolithography techniques to create microparticles with fine features and spatial patterns. A notable example in this regard is the “stop-flow lithography” developed by Doyle and co-workers, which involves flowing precursor solutions within a microfluidic channel.<sup>31</sup> Short exposure of the precursor flow to UV light under a photo-mask creates discrete,

individual microparticles, while fine sub-micron patterns can be transferred from the photo-masks to the bodies of these microparticles.

### **2.5.3. Chemical Crosslinking**

Microfluidic droplets can be crosslinked by contact with reactive chemicals present in the continuous phase. For example, consider the microfluidic generation of alginate microparticles. Alginate is a polysaccharide that undergoes ionic crosslinking upon contact of its L-guluronic repeat units with divalent ions like  $\text{Ca}^{2+}$ . An aqueous solution of alginate along with nano-sized  $\text{CaCO}_3$  particles is first dispersed into discrete droplets in a microfluidic chip. Then a pH change induced by acetic acid present in the continuous (Oil) phase is used to release  $\text{Ca}^{2+}$  ions from the nanoparticles, resulting in crosslinked alginate microparticles.<sup>32</sup> In Chapter 3, we present an example of such chemical crosslinking, where droplets of the polysaccharide, chitosan are solidified by glutaraldehyde in the continuous phase. Glutaraldehyde is a bi-functional crosslinker for polymers containing primary amines in their repeat units, with the aldehyde groups forming covalent bonds with these amine groups.<sup>33</sup>

The diffusion of the reactive chemical controls the morphology and texture of the microparticles. If diffusion is slow or the diffusion time is limited, chemical crosslinking is mostly confined to the outer surface of the droplet.<sup>34</sup> The resulting microparticles are composed of a solid shell and a liquid core and are called “microcapsules”. In contrast, if the chemicals diffuse rapidly through the entire droplet, it results in microparticles with a uniform, solid texture, which are then termed “microbeads”.

## 2.6. FABRICATION OF MICROFLUIDIC DEVICES

Herein, we present a general overview of commonly used microfluidic fabrication techniques.

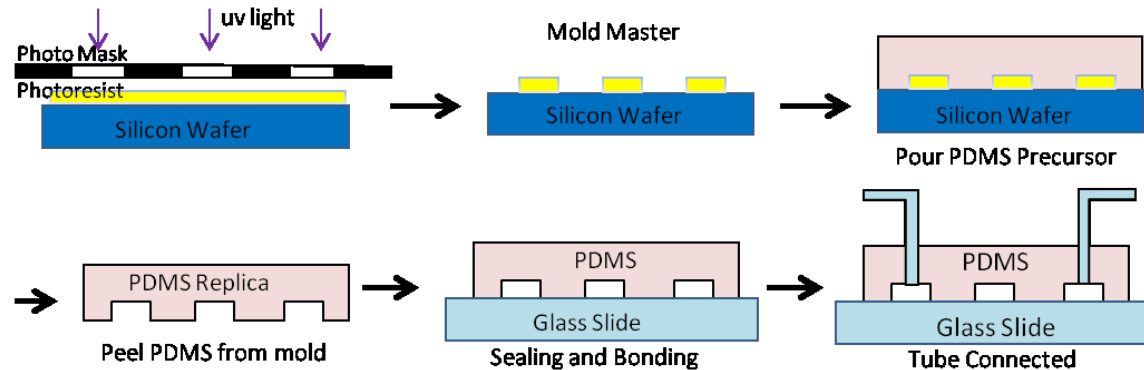


**Figure 2.3.** Schematic illustration of typical fabrication procedures for microfluidic devices via PDMS soft lithography.<sup>20</sup>

### 2.6.1. PDMS Soft Lithography

Polydimethylsiloxane (PDMS) soft lithography was first introduced by the group of Whitesides and soon became the standard fabrication technique for microfluidic systems.<sup>35</sup> This is because of its simplicity, versatility, and reliability. Basically, it involves creating replicas of a soft polymeric mold from an original hard master (Figure 2.4). Typical hard masters can be produced by standard photolithography.<sup>35</sup> With the hard master prepared, the soft replica can be produced by pouring a mixture of curable PDMS precursors onto them. In most cases the Dow Corning Sylgard 184 PDMS kit is used, which consists of two parts, a base and a curing agent, mixed at a mass ratio of 10:1. After curing, the PDMS replica is removed from the master, and is subsequently bonded to another cover slip to tightly close the gap. For applications that do not require a strong bonding strength, additional surface treatment may not be needed as the interaction

between the PDMS replica layer and cover plate would be strong enough to seal these microchannels. However, if rigorous operation is required, additional surface treatment such as by oxygen plasma is needed to permanently seal the two layers. After bonding, interface holes that provide connections to external tubing (to allow liquid injection) can be produced by pushing through the PDMS layer with a sharp puncher.

Aside from the simplicity in fabrication, it should also be noted that PDMS devices produced through soft lithography have low background fluorescence and excellent biocompatibility. This allows these devices to be widely used in many chemical and biological applications. However, PDMS devices are generally less tolerant of organic solvents due to the significant permeability and swelling of the polymer.

### **2.6.2. Thermoplastic Microfabrication**

Thermoplastic polymers can be used as substrates for microfluidic devices.<sup>36</sup> Microchannels in thermoplastics can be created through two methods: 1) hot embossing and 2) direct machining (Figure 2.5). In hot embossing, the thermoplastic substrate is pressed into a hard mold with protruding patterns at elevated temperatures where the thermoplastic is in a softened or melted state. Subsequent rapid cooling fixes the patterns from the mold into the substrate. Direct machining is done using techniques such as laser ablation and mechanical micro-milling. After microchannels are created, thermoplastic substrates need to be capped with a plain cover plate. Various bonding methods, such as adhesive, solvent, and thermal bonding, have been developed for this. An ideal bond interface should provide excellent seal without any layer delaminating during usage.

After bonding, world-to-chip interconnections can be built by inserting needles or tubing into mating holes drilled into the substrates.

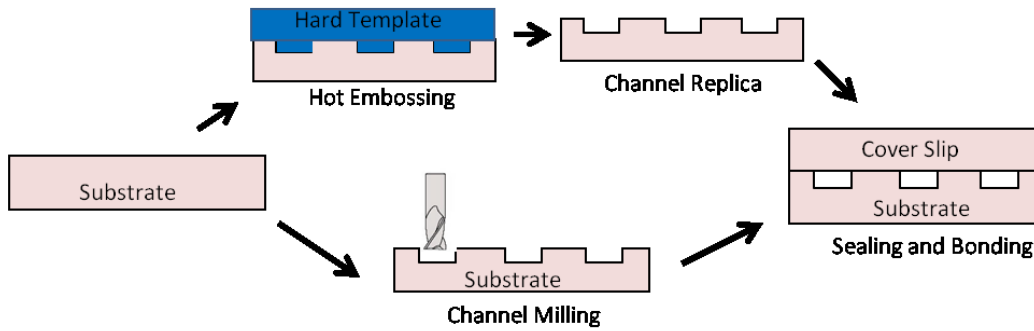


**Figure 2.4.** Schematic illustration of the fabrication routes of thermoplastics microfluidic devices. Top route: hot embossing method; bottom route: direct micro-machining.

Fabrication of microfluidic devices from thermoplastic substrates can be significantly more efficient and cost-effective than PDMS soft lithography. Thermoplastics costs are at least 100 times lower than PDMS. For small volume production, thermoplastic channels with dimensions approaching 50  $\mu\text{m}$  can be directly machined by micro-milling, obviating the need for photolithographic mold production, elastomer casting, and polymer curing. For mid-volume production, thermoplastics can be rapidly patterned by embossing from a micro-machined mold with cycle times on the order of 10 min, while high-volume production can be achieved using very low-cost reel-to-reel tape embossing methods.<sup>33</sup>

### 2.6.3. Capillary Tubing Devices

While microfluidic devices made by PDMS soft lithography or thermoplastic micromachining offer many advantages, they are still expensive and time consuming to

fabricate, especially for labs without expertise in microfabrication techniques and access to clean rooms. A simpler alternative does exist, and this involves manual assembly of glass capillaries into microdevices.<sup>22</sup> In a typical scheme (Figure 2.6), a glass capillary with a circular cross-section is heated and pulled to generate a fine orifice using a micropipette puller. The size of the orifice and its position can be adjusted by changing parameters on the capillary puller. The capillary is then inserted into an outer square glass capillary to form a co-axial assembly. Axisymmetric alignment of the two capillaries can be ensured by dimensional matching of the outer diameter of the inner circular capillary to the inner dimension of the outer square capillary. After assembly, epoxy glue is used to seal the gap between the inner circular capillary and outer square tubing. Plastic tubing can also be attached to these capillaries so that liquids can be introduced.<sup>22</sup> This approach greatly minimizes the time, cost, and effort for device fabrication as all the components are commercially available. Since the capillaries are made of glass, the wetting properties of their surfaces can be easily modified to be either hydrophilic or hydrophobic by treatment with appropriate silane modifiers.

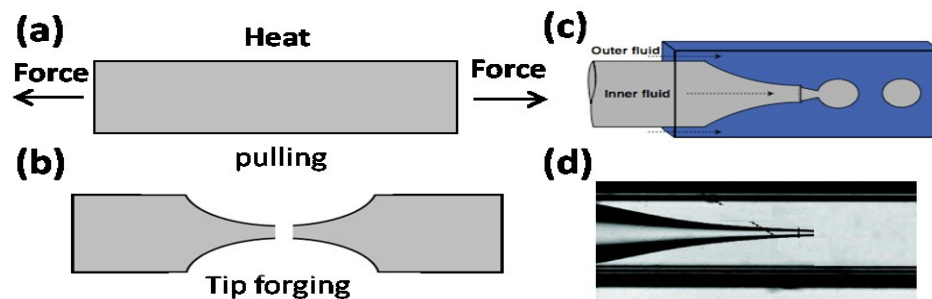


**Figure 2.5.** Schematic illustration of procedures for droplet generator assembled from capillaries. (a) capillary pulling under heat; (b) breakage of the pulled tip via microforging; (c) assembled microdroplet generator;<sup>22</sup> (d).microscopic image of such a device.<sup>37</sup>

## Chapter 3

# MICROFLUIDIC PRODUCTION AND ASSEMBLY OF CHITOSAN MICROPARTICLES\*

### 3.1. INTRODUCTION

The vision of “bottom-up” micro-manufacturing involves manipulating and precisely positioning individual building blocks (subunits) into more complex, higher-order assemblies. <sup>[38-53]</sup> For bottom-up micro-assembly to be realized successfully, subunits have to be carefully defined, appropriate assembly methods must be chosen, and reliable techniques have to be developed for linking subunits together. In recent years, a variety of approaches have been put forward to produce micro-assemblies with defined geometries, patterns, compositions, and functional attributes. <sup>38-53</sup> These studies have typically used prefabricated colloidal particles as the subunits, with alignment and positioning of these subunits into designed assemblies accomplished with the help of external forces and/or confined spatial templates. Additionally, stable connections between individual subunits in a given assembly have been achieved by using chemical crosslinkers,<sup>38</sup> biomolecular interactions,<sup>39,42</sup> or thermal fusion.<sup>52-53</sup> However, the use of prefabricated subunits limits both the level of manufacturing integration and the functional capabilities of the resulting assemblies. For example, the use of solid particles prevents the incorporation of additional encapsulants into the final assemblies. Also, the

---

\* The results presented in this chapter have been published in the following journal article: Jiang K.Q., Xue C., Arya C.D., Shao C.R., George E.O., DeVoe D.L., Raghavan S.R. A New Approach to In-Situ "Micromanufacturing": Microfluidic Fabrication of Magnetic and Fluorescent Chains Using Chitosan Microparticles as Building Blocks. *Small* **2011**, 7, 72470-2476.

use of thermal fusion to fix the subunits necessitates complicated device requirements while also being incompatible with the integration of biologically-active components. Similarly, the use of chemical crosslinkers to connect prefabricated subunits demands that chemical handles be available on the subunits, thereby constraining the range of possible subunit materials or necessitating additional pre-processing steps with the subunits. To overcome these limitations, new techniques are needed that enable facile generation of subunits as well as their subsequent connection within an assembly.

Recently, microfluidics has emerged as a promising platform for the synthesis and assembly of microscale particles. While much research has been focused on the generation of microparticles,<sup>32,34,54-57</sup> microfluidics can also provide a potential manufacturing paradigm at the microscale.<sup>49-53</sup> First, nearly monodisperse subunits with precise and tunable size can be generated in a continuous process,<sup>58</sup> and different payloads can be readily encapsulated within these subunits.<sup>32,55-57</sup> Confined microfluidic channels can provide ideal spatial templates to anchor these subunits into complex assembly patterns, with stable intra-particle interactions achieved through the application of chemical or physical inputs.<sup>49-53</sup> Moreover, the continuous nature of microfluidic particle generators offers the potential of realizing subunit generation, functionalization, and assembly all within a single microfluidic chip.

In this chapter, we present a microfluidic scheme that can both produce micro-sized subunits and also connect these subunits within the same chip into complex multi-particle configurations. To illustrate the types of connected structures that can be

produced, we focus on 1-dimensional chains. Our subunits are microparticles of the biopolymer, chitosan. This amino-polysaccharide has been intentionally selected because its primary amines allow for both intra-particle and inter-particle cross-linking upon contact with dialdehydes like glutaraldehyde (GA).<sup>59</sup> We first generate monodisperse droplets by contacting an aqueous solution of chitosan at a microfluidic T-junction with a stream of hexadecane containing the detergent Span 80.<sup>58</sup> These droplets are then interfacially crosslinked by a solution of GA injected through a tertiary channel. Robust chitosan microparticles of defined size are thus produced, and the functional properties of these particles are easily varied by including various payloads along with the chitosan solution, such as magnetic nanoparticles (MNPs) of  $\gamma\text{-Fe}_2\text{O}_3$  and fluorescent water-soluble dyes.

We then demonstrate on-chip assembly of individual microparticles into permanent connected microchains. Here, we use the downstream microchannel as a spatial template to confine the particles, and GA again serves as the chemical “glue” to link amine moieties on chitosan chains from adjacent particles. This allows us to generate chains of magnetic and/or fluorescent particles. Key notable points about our approach are the ability to control chain length with precision and the ability to control the arrangement of particles within a chain, e.g., to generate chains with alternating fluorescent and non-fluorescent particles. In addition, chain flexibility can also be tuned by modulating the extent of GA-based crosslinking of adjacent particles (via the incubation time). Accordingly, we have created both rigid magnetic chains that can be rotated by an external magnetic field as well as semiflexible magnetic chains that show a

beating motion in response to a magnetic field. Such magnetic chains are of interest for a variety of applications, e.g., as micromixers in microscale devices, as drug delivery vehicles for magnetically targeted delivery, or as biomimetic microrobots.<sup>38-39,41-42</sup>

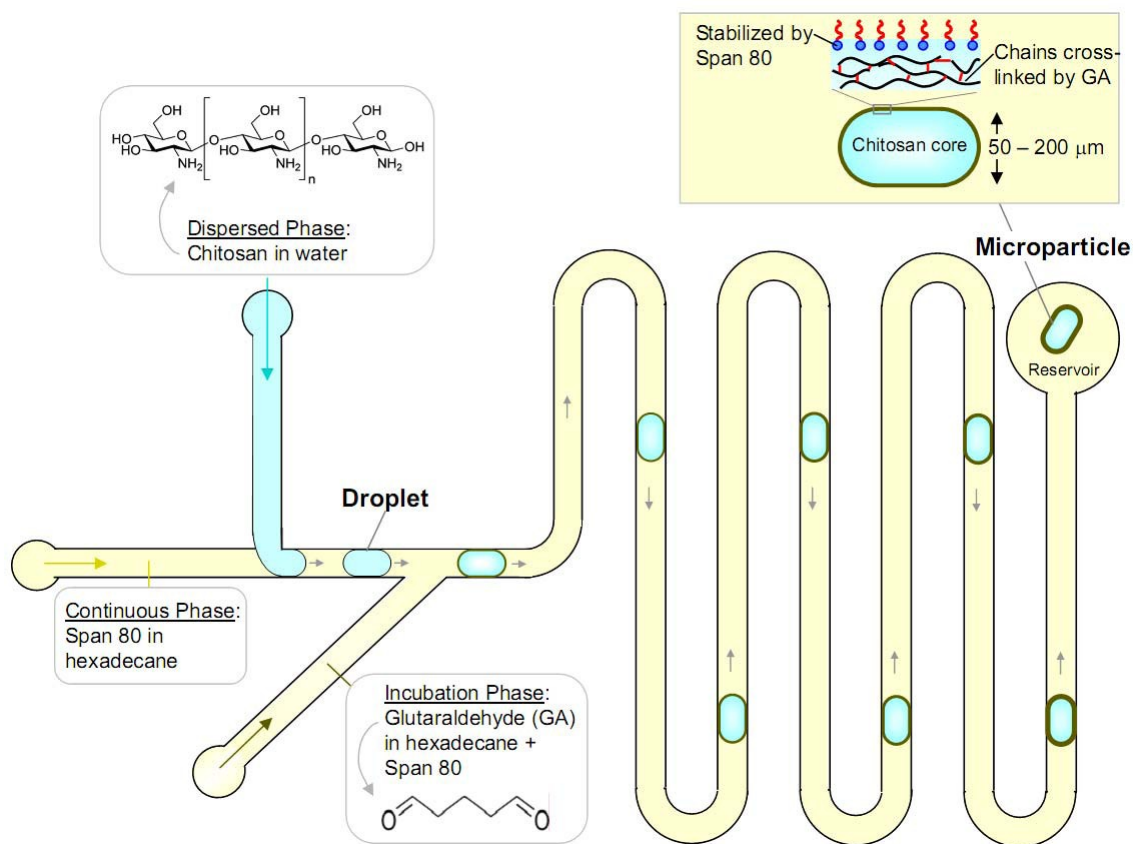


**Figure 3.1.** Microfluidic generation of chitosan microparticles. The channels have a rectangular cross-section (125  $\mu\text{m}$  height and 100  $\mu\text{m}$  width). At the T-junction, the dispersed phase (an aqueous chitosan solution) is contacted with the continuous phase (a solution of the detergent, Span 80 in hexadecane), and in turn, discrete aqueous droplets are formed. These droplets travel down the channel and meet the flow of the incubation phase, which consists of glutaraldehyde (GA) emulsified in hexadecane using Span 80. The GA crosslinks the droplets as they travel through the long, serpentine channel segment. Ultimately, the droplets are converted into particles and these are collected in the reservoir at the end. The inset shows a single microparticle: note that the chitosan chains are covalently linked by GA and the particle is stabilized in hexadecane by detergent molecules.

Overall, our approach is distinct from other microfluidic manufacturing routes in that both subunit generation and subsequent connection are accomplished on the same chip and using the same chemistry. In contrast, in other approaches, subunit generation and assembly are usually carried out in separate steps with different chemistries in each step. Also, it should be noted that the chemicals used in this work are low-cost and commercially available, and no additional synthesis or purification steps are used. Finally, our microfluidic devices are based on the thermoplastic poly-methyl-methacrylate (PMMA), which makes the devices relatively cost-effective and easy to fabricate compared to those prepared from other substrate materials such as glass and polydimethylsiloxane (PDMS).<sup>60-62</sup> Thus, the above “micro-manufacturing” process can potentially be scaled up for high-throughput production.

### 3.2. EXPERIMENTAL SECTION

**Materials and Chemicals:** Chitosan (medium molecular weight, 190–310K; degree of deacetylation ~ 80%) was obtained from Sigma-Aldrich. Magnetic  $\gamma$ -Fe<sub>2</sub>O<sub>3</sub> nanoparticles (average surface area ~ 42 m<sup>2</sup>/g) were purchased from Alfa Aesar. The water-soluble fluorescent dye, sodium-fluorescein; the nonionic detergent, sorbitan-monooleate (Span 80); the nonpolar solvent, hexadecane; and the crosslinking reagent, glutaraldehyde (grade I, 50%) were obtained from Sigma-Aldrich. All chemicals were used as received. Rectangular neodymium bar magnets were obtained from McMaster Carr and nylon net filters (pore size, 30  $\mu$ m) were purchased from Millipore.

**Solution Preparation:** Chitosan (2 wt%) was dissolved in a acetic acid (0.2 M) solution. For magnetic and fluorescent capsule generation,  $\gamma$ -Fe<sub>2</sub>O<sub>3</sub> nanoparticles (0.5 wt%) and sodium fluorescein(0.1 wt%) were added to this solution, followed by vortex mixing and sonication. The final mixture is referred to as the “dispersed” phase. The “continuous” phase was prepared by dissolving Span 80 (2 wt%) in hexadecane. Finally, the “incubation” phase was a solution in hexadecane containing Span 80 (2 wt%) and glutaraldehyde (2 wt%). The above mixture was vortexed and sonicated before use.

**Microfluidic Chip Fabrication and Operation:** The microfluidic chip comprised a PMMA substrate (4" x 2" x 1/16") containing microchannels bonded to a PMMA lid having access ports.<sup>62</sup> PMMA sheets (FF grade; 4" x 4" x 1/16") were purchased from Piedmont Plastics. The microchannels were fabricated by mechanical milling using a end mill (125  $\mu$ m diameter) on a CNC milling machine with a depth of 100  $\mu$ m. Holes for the needle interface and access reservoir were drilled into the substrate plate using a 650  $\mu$ m diameter drill bit and a 2 mm diameter drill bit, respectively. The machined PMMA plate was sequentially cleaned by DI water and isopropyl alcohol to remove the milling debris, followed by a 24 h degassing step in a 40 °C vacuum oven to remove the residual solvents. After vacuum drying, both the processed PMMA and a raw PMMA chip were oxidized by an 8 min exposure to ultraviolet (UV) light in the presence of ozone.<sup>60</sup> The oxidized PMMA wafers were immediately mated together and thermally bonded at 85 °C in a hot press under a pressure of 3.45 MPa for 15 min. The world-to-chip interfaces were established by inserting hypodermic stainless steel needles into the 650  $\mu$ m diameter mating holes, with an additional 30 min of annealing at 85 °C to release the residual

stresses from the fitting process.<sup>63</sup> Commercial microfluidic fittings (Upchurch) were used to connect the needle ports on the PMMA chip with off-chip fused silica capillaries, which were further connected to syringes. Precision syringe pumps (PHD 2000, Harvard Apparatus) were used to control the infusion of fluids into the chip. Optical detection was performed using either a Nikon Eclipse LV-100 Profilometer Microscope or a Nikon Eclipse TE2000S inverted fluorescence microscope.

### **3.3. RESULTS AND DISCUSSION**

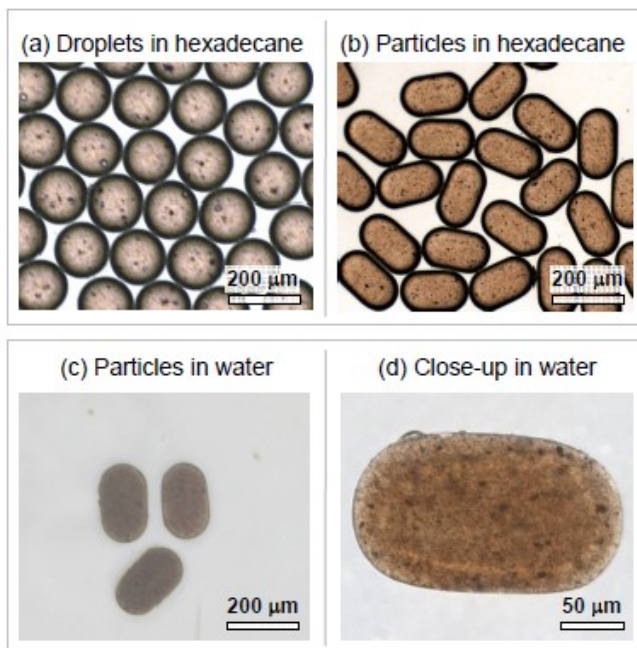
#### **3.3.1. Droplet Generation and Conversion to Robust Microparticles**

Figure 3.1 shows a schematic of our microfluidic apparatus. The first element is the T-junction where the aqueous dispersed phase (2 wt% solution of chitosan) comes in contact with the non-polar continuous phase (2 wt% solution of the detergent, Span 80 in hexadecane). As the dispersed phase is forced into the continuous phase, shear forces break up the aqueous stream into a series of equally spaced droplets.<sup>58</sup> The droplets are stabilized in the non-polar continuous phase by Span 80 molecules, which are expected to arrange at droplet surfaces with their polar heads oriented inwards and their non-polar tails pointing outwards into the external liquid (Inset in Figure 3.1). The droplet size and generation frequency can be tuned to a desired value by adjusting the flow rates of the continuous and dispersed flows, or by adjusting the size of microfluidic channel.<sup>58</sup> In the present work, flow rates of 1.5  $\mu\text{L}/\text{min}$  for the continuous flow and 0.3  $\mu\text{L}/\text{min}$  for the dispersed flow were used to produce  $\sim 150 \mu\text{m}$  diameter droplets, with a typical generation speed of 1 droplet per second. This relatively slow generation rate was chosen

to simplify the overall control of the system. However, higher generation speeds can be readily achieved within the same device by adjusting the total flow rates.

The second element in our microfluidic setup is the “incubation” stream, which is delivered through a side-channel downstream from the T-junction to contact the droplets passing through the main channel (Figure 3.1). The incubation phase contains 2 wt% of glutaraldehyde (GA) emulsified into hexadecane using 2 wt% of Span 80 detergent. Note that GA is a bifunctional molecule, well-known for its ability to react with the amine groups of chitosan and thereby crosslink chitosan droplets.<sup>59</sup> When a chitosan-bearing droplet contacts the GA stream, GA molecules diffuse to the droplet and crosslink or “fix” the chitosan chains therein (Inset in Figure 3.1). Similar crosslinking of droplets has been studied by Kumacheva et al<sup>34,55</sup> for the case of alginate droplets in the presence of  $\text{Ca}^{2+}$  ions diffusing from the oil phase – the morphology of the resulting particles generally correlates with the concentration of crosslinkers. At low levels of crosslinker, the reaction is confined to the outer surface of the droplet and the resulting particle assumes a core-shell “microcapsule” structure. At higher levels of crosslinker, the entire droplet gets crosslinked and the particle is termed a “microbead” or “microgel”. For the case of our chitosan/GA system, we have observed that the contact (incubation) time between GA and chitosan droplets has a strong influence on the robustness of the resulting particles. To increase the incubation time, we position a long serpentine channel segment downstream from the GA injection point. For typical flow rates of 1.5  $\mu\text{L}/\text{min}$  for both the continuous and incubation streams (corresponding to  $\sim 1$  droplet/second), an incubation time of  $\sim 3$  min was found to be sufficient to convert the droplets into robust

microparticles. The microparticles were then collected from the reservoir located at the end of the incubation channel.



**Figure 3.2.** Optical micrographs of: (a) spherical chitosan-bearing aqueous droplets in hexadecane (these were not contacted with GA); (b) plug-like microparticles formed by crosslinking the above droplets with GA; (c) the above microparticles transferred from hexadecane to deionized water, and (d) close-up of a single microparticle in water. Note that the droplets/particles contain MNPs, and the black spots in the images correspond to aggregates of these MNPs.

Besides their robustness, another interesting aspect of our microparticles is their geometrical anisotropy. Generally, when the droplets emerge from the T-junction, they are deformed into a plug-like shape due to the constraint placed by the channel walls. In the absence of GA-crosslinking, the droplets regain their surface-minimizing spherical form once they fall into the reservoir. A bright-field optical micrograph of uncrosslinked droplets collected in the reservoir and surrounded by the continuous phase of hexadecane is shown in Figure 3.2a. Note that the droplets are spherical and also note their low

polydispersity. However, when the plug-like droplets are brought into contact with GA in the channel, the rapid crosslinking fixes their anisotropic shape and the resulting particles do not relax back into a spherical form in the reservoir. This is seen from Figure 3.2b, which is a micrograph of GA-crosslinked microparticles in hexadecane. In addition, these crosslinked particles are stable enough to be transferred from hexadecane to deionized (DI) water, which is an important virtue for applications where compatibility with aqueous solutions is necessary. The transfer was done by filtering the contents of the reservoir through a nylon net filter (30  $\mu\text{m}$  pore size), followed by rinsing of the residue with ethanol and DI water, and finally adding the rinsed residue into DI water. Figure 3.2c is a micrograph of microparticles in DI water, and a close-up of a single particle is shown in Figure 3.2d. Note that these particles contained MNPs, and the black spots in the image correspond to aggregates of the MNPs. We have also conducted SEM on the chitosan microparticles. The particles appear to be relatively homogeneous, suggesting that they are closer to microgels rather than microcapsules. Attempts to examine fracture surfaces by SEM were inconclusive, and this aspect requires further investigation.

### **3.3.2. Linking Microparticles into Microchains**

Next, we describe our method for linking microparticles into chains. This method relies on the spatial confinement of particles in a microfluidic channel and GA-chitosan crosslinking to connect adjacent microparticles. We flow the microparticles into a channel and use a stainless steel wire ( $\sim 60 \mu\text{m}$  diameter) to partially block the channel outlet (Figure 3.3a). The particles are thus trapped within the channel while the flow of solution around them continues. To avoid excessive pressure buildup, we stop the

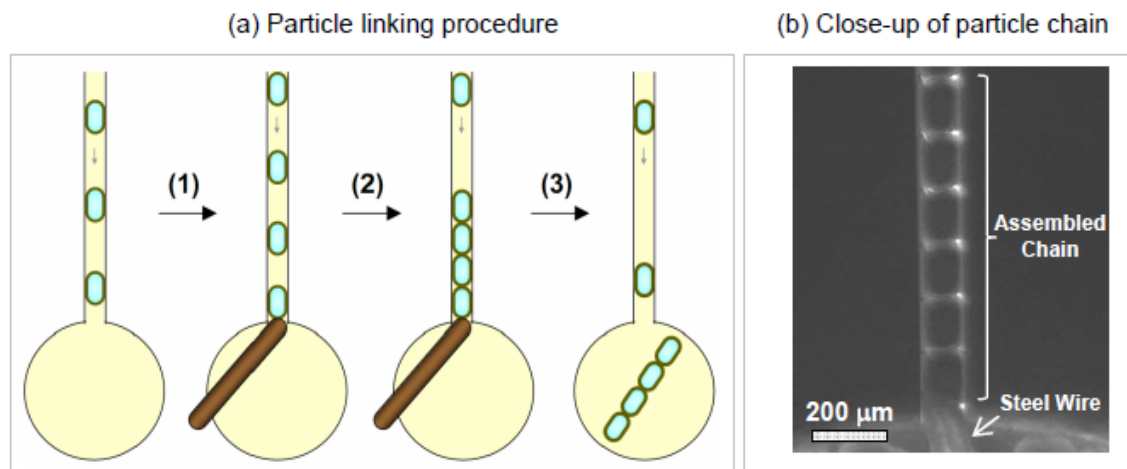


**Figure 3.3.** (a) Schematic depiction of the on-chip process for linking individual particles into chains. (1) A stainless steel wire is used as a valve to block the channel outlet, (2) the wire is held until the desired number of subunits has been accumulated on the chain, and (3) the wire is then removed and the chain is flushed into the reservoir. (b) Optical micrograph showing a close-up of the assembled chain inside the microchannel.

continuous and dispersed flows and reduce the incubation flow rate to  $0.03 \mu\text{L}/\text{min}$ . Successive microparticles are allowed to add onto the tail of the growing chain until the desired chain length is reached. In the process, individual subunits are brought into close proximity, allowing GA to form inter-particle covalent bonds between chitosan chains on each pair of adjacent particles. Figure 3.3b is an optical micrograph showing a particle chain in the channel. The extent of coupling between particles is determined by the GA-contact time (i.e., the time over which the channel outlet is blocked). The flexibility of the chain can be controlled by varying this contact time, as further discussed in the next section. A key feature of our approach is the control over chain length. When the desired number of subunits has been connected into a robust chain, the chain is flushed into the reservoir, as shown in Figure 3.3a. We have found that a contact time of 5 min is

sufficient to form a robust chain that does not fall apart in the reservoir. The above process can be easily replicated to generate multiple chains possessing precise lengths.

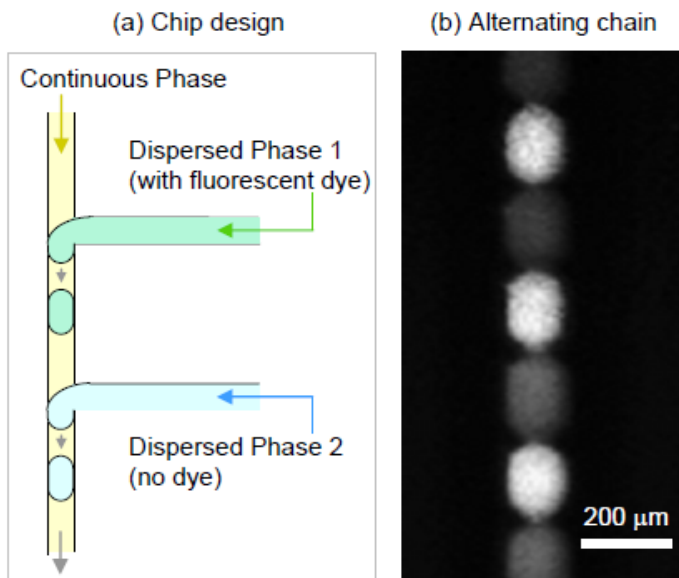


**Figure 3.4.** (a) Schematic of the modified chip design used to prepare chains of alternating particles. The chip has two T-junctions, corresponding to two dispersed phases. One dispersed phase has 0.1% of the fluorescent dye, sodium fluorescein while the other does not contain dye. When the flow rates of the two dispersed phases are set equal, an alternating sequence of drops with and without the dye travel down the channel, where they are fixed into chains as described in Figure 3.3. (b) Fluorescence micrograph showing a particle chain with alternating fluorescent and non-fluorescent subunits.

Furthermore, we demonstrate the ability to combine multiple building blocks within the same structure with precise control over their subunit arrangement. For this we modified the design of our microfluidic chip to feature two inlets for different dispersed phases (Figure 3.4a). We used a mixture of 2% chitosan and 0.1% of the water-soluble fluorescent dye, sodium fluorescein for dispersed phase 1 whereas dispersed phase 2 contained 2% chitosan only. When the flow rates of the two dispersed phases are the same (typical value: 0.3  $\mu\text{L}/\text{min}$ ), the microparticles flowing down the main channel

alternate between fluorescent and non-fluorescent ones. Such a microparticle train was blocked off, as shown before in Figure 3.3a, by the steel wire to enable inter-particle connections to form during contact with GA. This process eventually results in a connected chain of alternating subunits. The alternating structure is clearly seen from the fluorescence micrograph in Figure 3.4b, where every second subunit in the chain shows bright fluorescence compared to its nearest neighbors. Other variations in chain structure, e.g., where every  $n$ th microparticle in the chain is fluorescent, can also be prepared by simply controlling the relative flow rates of the two dispersed phases.

### **3.3.3. Magnetic Chains of Varying Flexibility**

To further illustrate the possibilities inherent in our approach, we focus on a specific payload of interest, viz. MNPs of  $\gamma$ -Fe<sub>2</sub>O<sub>3</sub>. By encapsulating MNPs, we can impart magnetic properties to the individual microparticles. Towards this end, we mixed in 0.5 wt% of the MNPs with the 2 wt% chitosan solution and used this mixture as the dispersed phase. Interestingly, the MNPs did not remain well-dispersed for long times in the chitosan solution – the fluid appeared homogeneous but microsized clumps could be seen by optical microscopy (as noted in Figure 3.2d). The clumping could be minimized by vigorous sonication of the dispersed phase before injection into the microfluidic device. At any rate, once the MNPs were encapsulated in the core of the chitosan microparticles, the clumping was not an issue with regard to the magnetic behavior of the microparticles. We confirmed that individual microparticles containing the MNPs could be magnetically manipulated using external bar magnets.

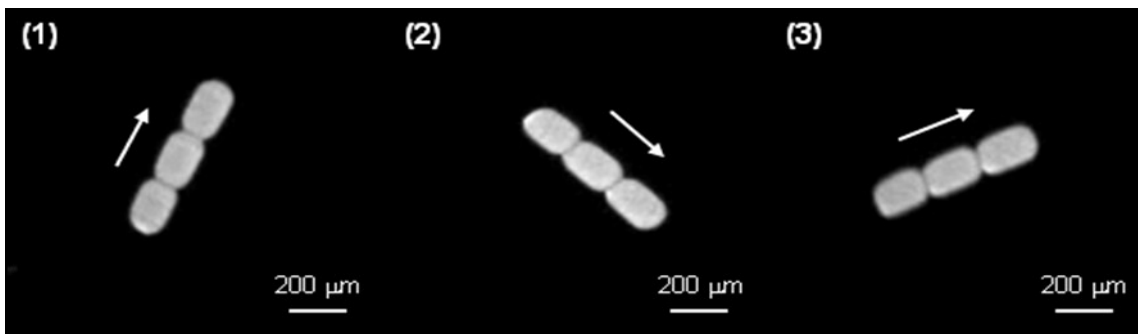


**Figure 3.5.** Rotation of a rigid magnetic chain when a bar magnet is rotated above the holding container. The chain is formed by extensive fusion of three chitosan particles bearing MNPs and a fluorescent dye. (1) to (3) represent successive images taken using a fluorescence microscope. Arrows indicate the direction of the net (induced) magnetic dipole at each instant.

We then proceeded to create chains of magnetic particles using the procedure described above. First, we made stiff chains – in this case, the assembly was incubated for 24 h inside the channel to allow extensive inter-particle connections via GA. The magnetic response of a stiff, three-member long magnetic chain is demonstrated in Figure 3.5 (these subunits also contained the fluorescent dye and the images are taken with a fluorescence microscope). For these experiments, the chain was transferred out of the microchannel and was placed in a petri dish. A permanent bar magnet was positioned a few centimeters above in an orientation parallel to the chain. When the external magnet was rotated from its original axis, the particle chain correspondingly rotated, as shown in Figure 3.5. Note that the assembled chain itself does not possess an intrinsic dipole to enable rotational control. Instead, the process results from interactions between the encapsulated MNPs. Under a constant magnetic field, each MNP establishes an individual magnetic dipole aligned to the applied field. Interactions between these dipoles generate a distribution of forces that exert a net torque on the chain until the chain's axis

is aligned to the applied field. Similarly, translational motion of the magnetic chain may be realized by positioning one pole of the bar magnet closer to the assembled chain than the opposite pole. The magnetic control of longer rigid chains containing 30~40 subunits has also been realized.

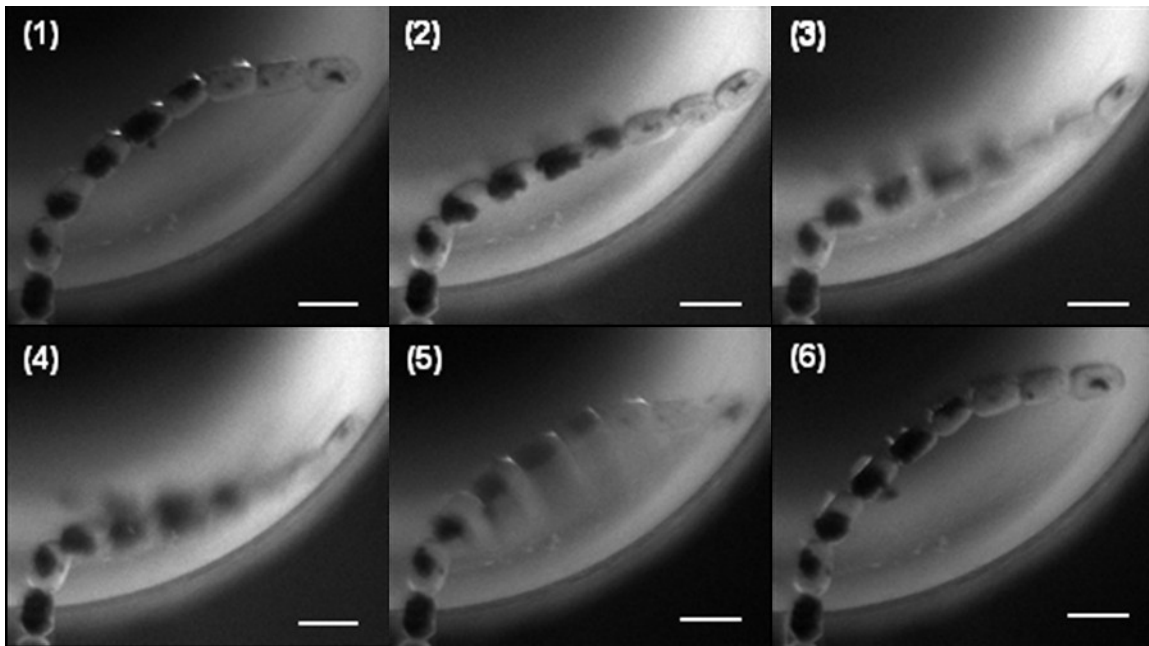


**Figure 3.6.** Undulating or “beating” motion of a semiflexible magnetic chain when a magnet is swayed on top of the holding container. (1) to (6) represent successive images obtained using a bright-field optical microscope. Scale bars in all images are 200  $\mu\text{m}$ .

The stiffness of the fabricated chains can be controlled by adjusting the contact (incubation) time of the chitosan microparticles with GA inside the blocked channel. Note that GA enhances both the degree of intraparticle crosslinking, which dictates the inherent modulus of the resulting chain, and the degree of interparticle cross-linking, which defines the rigidity of the interface between adjacent particles. While the relative influence of these factors is still under investigation, it is clear that long incubation times (~ 24 h) lead to stiff rod-like chains, as shown above. In contrast, a moderate incubation

time of  $\sim 5$  min produces flexible but mechanically robust chains. As illustrated by Figure 3.6, such semiflexible magnetic chains exhibit an undulatory (“beating”) motion when the orientation of an external magnetic field is changed.

### **3.3.4. Future Outlook**

The broad approach of microfluidic assembly presented in this paper can be extended in a number of ways. For example, one could vary the net magnetic property of a chain by alternating magnetic and non-magnetic subunits or by having every fifth or tenth unit be a magnetic microparticle. One could also make chains of microparticles that are both magnetic and fluorescent to varying degrees, such as a chain with alternating magnetic and fluorescent units. Such an alternating arrangement of subunits may be of interest in the context of chemical and biological sensing.<sup>19</sup> Lastly, in addition to linear chain assemblies, a variety of other shapes can be constructed using our microfluidic approach. One example is a Y shape of connected microparticles, which can be formed by branching the main channel into two and blocking off these branches to allow inter-particle linking. This and other structures are being studied as part of ongoing work in our laboratory and will be reported in future papers. We believe our overall assembly approach of using chitosan microparticles as building blocks and connecting them with precision into larger structures is likely to be of considerable interest among scientists and engineers.

## **3.4. CONCLUSIONS**

We have formed soft microparticles within a microfluidic device by contact of chitosan-bearing aqueous drops with a mixture of GA in hexadecane. These particles

have low polydispersity and can be redispersed into DI water. Microparticle properties can be readily altered by varying the payloads included along with the initial chitosan solution: here, by using MNPs and fluorescent dyes we obtain magnetic and/or fluorescent particles. We then use these particles as building blocks for the construction of chains. To form chains on-chip, the microparticles are brought into close contact within a microchannel and incubated with a GA solution, whereupon the GA covalently links chitosan chains from adjacent particles. The chain length as well as the arrangement of particles within a chain can be precisely controlled. Chain flexibility can also be tuned via the incubation time of the chain with GA – both rigid and semiflexible magnetic chains have been prepared by this approach. Overall, we suggest that microfluidic chips could serve as futuristic micro-manufacturing platforms in which building blocks could both be synthesized and then subsequently connected and positioned into complex and useful structures.

## Chapter 4

# MONODISPERSE PDMS MICROBEADS AS DISCRETE OXYGEN SENSORS\*

### 4.1. INTRODUCTION

Microfluidics has emerged as a powerful platform for the generation of microparticles with tailored structure and properties.<sup>14,57</sup> While the microfluidic synthesis of a variety of microparticles has been demonstrated, a particularly interesting polymer for microparticle production is poly(dimethylsiloxane) (PDMS). PDMS is an inert silicone elastomer that serves as a key component in a range of lubricants, sealants, and medical products, and is widely used in the fabrication of microfluidic chips using soft lithography techniques.<sup>64</sup> It is an attractive material for microparticle synthesis for several reasons. Siloxane surface groups presented by PDMS serve as convenient chemical handles for facile particle functionalization. Furthermore, the high permeability for various solvents and gases allows PDMS microparticles to readily absorb agents from the local environment, allowing the particles to serve as separation and sensing elements.

The production of uniform microscale PDMS beads by conventional (bulk) methods has proven to be challenging.<sup>65-67</sup> Bulk techniques for bead production usually

---

\* The results presented in this chapter have been published in the following journal article: Jiang K.Q., Thomas P.C., Forry S.P., DeVoe D.L., Raghavan S.R. Microfluidic synthesis of monodisperse PDMS microbeads as discrete oxygen sensors. *Soft Matter* **2012**, *8*, 923-926.

require the generation of stable emulsions of PDMS precursors in water. However, the high viscosities of typical PDMS prepolymer formulations together with the low surface energy of PDMS makes the generation of stable emulsions in aqueous solution rather difficult.<sup>67-69</sup> As a result, PDMS precursor droplets tend to aggregate or coalesce, especially during the high-temperature curing step required for converting these into crosslinked beads.<sup>68-69</sup> Such aggregation adversely influences the polydispersity and morphology of the final beads.

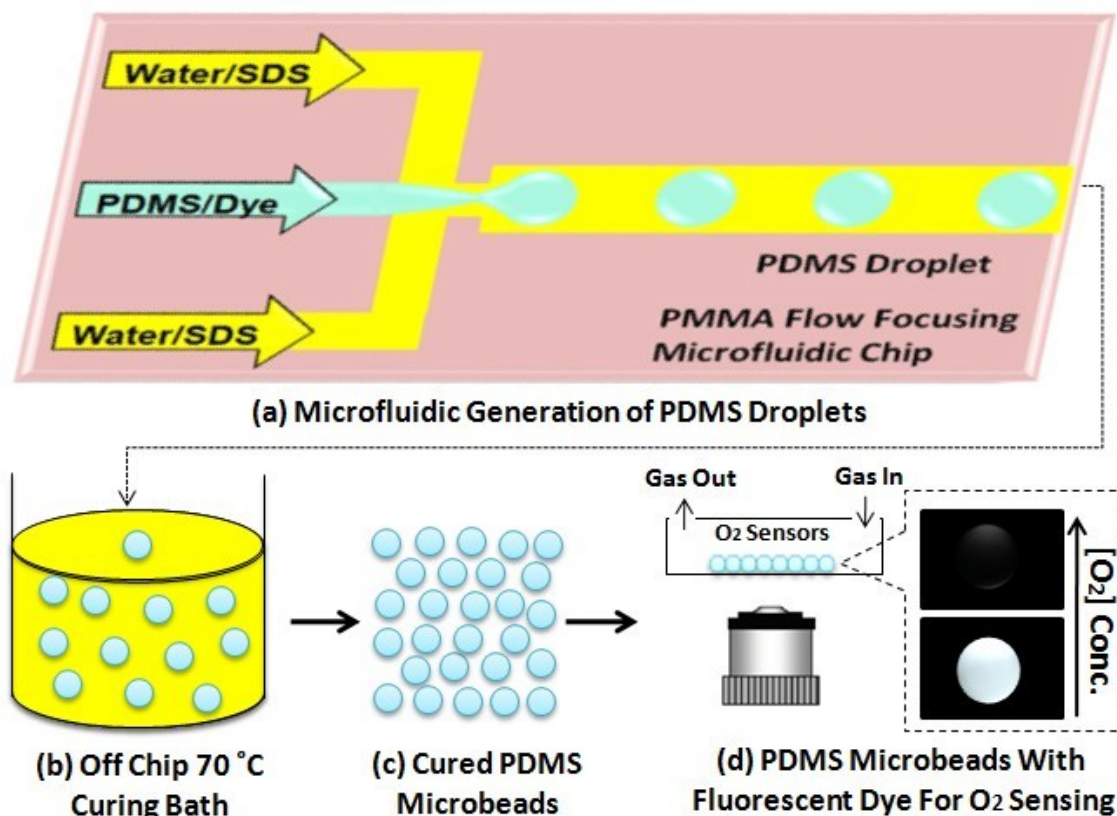


**Figure 4.1.** Illustration of the scheme for producing PDMS microbeads that can be used as oxygen sensors. (a) Microfluidic generation of PDMS droplets bearing a phosphorescent dye by flow-focusing on a PMMA microfluidic device; (b) Off-chip curing of the PDMS droplets at 70°C; (c) Rinsing and harvest of the resulting dye-bearing microbeads; (d) Use of these microbeads for oxygen sensing.

However, there are additional challenges associated with flowing PDMS precursors in microfluidic devices. Beyond the issues noted above for bulk emulsion generation, an additional constraint is that most microfluidic devices are commonly based on soft lithography where the microchannels themselves are fabricated from PDMS. In this case, it is difficult to disperse a flow of PDMS precursor into microdroplets due to the high affinity between the dispersed liquid and microchannel surfaces.<sup>18,70-71</sup> While this issue may be addressed by specifically engineering PDMS sidewalls by techniques such as UV-photografting,<sup>72</sup> vapor-phase deposition<sup>73</sup> or sol-gel coating,<sup>18,71</sup> these approaches are generally not ideal and involve complex processing methods. An alternate and preferable way to tailor wetting properties is by using other materials, such as thermoplastics, silicon, or glass, for the microfluidic substrate.

Here we report a new microfluidic strategy for the production of monodisperse PDMS microbeads, which addresses earlier concerns (Figure 4.1). We use a hydrophilic poly(methylmethacrylate) (PMMA) thermoplastic for the device substrate, and this prevents adhesion of PDMS droplets to channel walls. Within this device, we employ a flow-focusing mechanism to create droplets of PDMS precursors in an aqueous continuous phase bearing the surfactant, sodium dodecyl sulfate (SDS). The PDMS precursor solution is a mixture of two components, and we have carefully adjusted the ratio of these components, and thereby the viscosity of this solution. As a result, we are able to generate stable, non-coalescing droplets, and these are collected and thermally cured off-chip. Ultimately, we obtain a population of inert, monodisperse PDMS microbeads that could find application in a variety of areas. To advance applications, we

further exploit a valuable feature of our microfluidic approach, which is that payloads of interest can be easily embedded within the beads by simply combining with the initial PDMS solution. As an example that leverages the high gas permeability of PDMS and extends prior work using thin-film PDMS,<sup>74</sup> we demonstrate the integration of an oxygen-sensitive phosphorescent dye into the polymer microbead matrix. The resulting dye-bearing PDMS microbeads are shown to be capable of quantitatively sensing the concentration of oxygen in the surrounding medium in real time.

## 4.2 EXPERIMENTAL SECTION

**Materials and Chemicals:** The Sylgard 184 silicone elastomer kit was obtained from Dow Corning Corp as a free sample. The kit is composed of two fluids, Part A (base, consisting of vinyl-terminated siloxane oligomers) and Part B (curing agent, consisting of siloxane oligomers and catalyst). Sheets of thermoplastic polymethylmethacrylate (PMMA) (FF grade; 4" x 4" x 1/16") were purchased from Piedmont Plastics. The surfactant sodium dodecyl sulfate (SDS) was purchased from TCI America. The porphyrin dye Pt(II) meso-tetrakis(pentafluorophenyl) porphine (PtTFPP) was purchased from Frontier Scientific. All chemicals were used as received without any further treatment.

**Solution Preparation:** The continuous phase was prepared by dissolving 5 wt% of SDS in distilled-deionized (DI) water. The dispersed phase was a mixture of Sylgard Parts A and B at a weight ratio of 6:4. Mixing of these liquid parts was done by a vortex mixer, followed by bath sonication. For experiments with the dye, PtTFPP was first dissolved in

toluene and this solution was mixed with Sylgard Part A. The mixture was placed under vacuum overnight at 90 °C to evaporate the toluene (final concentration of PtTFPP in the mixture was 0.5 wt%). The above material was then mixed with the curing agent (Part B) at a 6:4 weight ratio.

**Microfluidic Device Fabrication and Operation:** The microfluidic chip comprised a PMMA substrate (4" x 2" x 1/16") containing microchannels bonded to a PMMA lid containing access ports. The smaller microchannels were fabricated by mechanical milling using a 50 µm diameter end mill on a CNC milling machine with a depth of 50 µm, and the bigger microchannel was milled using a 150 µm diameter end mill with a depth of 100 µm. Holes for the needle interface were drilled into the substrate plate using a 650 µm drill bit. The machined PMMA plate was sequentially cleaned by DI water and isopropyl alcohol to remove the milling debris, followed by a 24 h degassing step in a 40 °C vacuum oven to remove the residual solvents. After vacuum drying, both the processed PMMA and a raw PMMA chip were oxidized by an 8 min exposure to ultraviolet (UV) light in the presence of ozone. The oxidized PMMA wafers were immediately mated together and thermally bonded at 85 °C in a hot press under a pressure of 3.45 MPa for 15 min. The world-to-chip interfaces were established by inserting hypodermic stainless steel needles into the 650 µm diameter mating holes, with an additional 30 min of annealing at 85 °C to release the residual stresses from the fitting process. Commercial plastic PVC tubings were used to connect the needle ports on the PMMA chip with syringes. Precision syringe pumps (PHD 2000, Harvard Apparatus) were used to control the infusion of fluids into the chip. Typical infusion rates were 50 µL/min for the continuous phase and 1 µL/min for dispersed phase.

**Microbead Characterization:** Optical characterization of the beads was performed using either a Nikon Eclipse LV-100 Profilometer microscope or a Nikon Eclipse TE2000S inverted fluorescence microscope. Scanning Electron Microscopy (SEM) was done using a Hitachi SU-70 instrument. Beads were sputter-coated with a layer of gold for 90 s before SEM imaging. For the size distribution plot, data was obtained by measuring diameters for a population of 100 microbeads under the TE2000S microscope.

**Sensing Experiments with the Beads:** Dye-incorporated microbeads were placed in a modified multiwell plate equipped to allow continuous gas flow. Beads were exposed to gas with different partial pressures of oxygen ( $P_{O_2} = 0$  atm, 0.01 atm, 0.05 atm, 0.1 atm and 0.2 atm), which were obtained by mixing nitrogen and air. The emission intensity from the beads was captured on an inverted microscope (Zeiss Axiovert Z1, Thornwood NJ). A green LED (Thorlabs, Newton NJ) was used to illuminate the microbeads and images were captured using a CCD camera (CoolSnap HQ, Tucson AZ) with an integration time of 100 ms. All images were background corrected and analyzed using NIH Image J software(<http://rsbweb.nih.gov/ij/>).<sup>74</sup>

## **4.3. RESULTS AND DISCUSSION**

### **4.3.1. Microfluidic Production of PDMS Microparticles**

The first step in our scheme is the generation of discrete microscale droplets of PDMS precursor by microfluidic flow-focusing. In flow-focusing, a central nonpolar stream (dispersed phase) is brought into contact with two aqueous streams (continuous phase) from the side channels (Figure 4.2a).<sup>15,23</sup> The side flows spatially constrain the

central flow into a thin thread as they pass through the downstream orifice. On exiting the orifice, the central flow expands laterally, and a hydrodynamic instability ensues, causing break-up of this flow into a spherical droplet.<sup>15,23</sup> After break-up, the central flow retracts to the tip of the center channel and successive cycles of droplet production are repeated. It should be noted that in typical flow-focusing setups, the central flow (dispersed phase) is aqueous while the side flows are non-aqueous;<sup>14,57</sup> here, for our purpose, this order is necessarily inverted. The process of droplet generation by flow-focusing is known to be influenced by the viscosities of the two fluids, their interfacial tension, and the ratio of the continuous to dispersed flow rates.<sup>15,23,34</sup> For example, it is more difficult to disperse highly viscous fluids into individual droplets.<sup>23,34</sup> Viscous phases also cause an additional problem in that they require higher pressures to be applied for fluid injection. These pressures can exceed the capabilities of syringe pumps and could also cause delamination of the microfluidic chip.

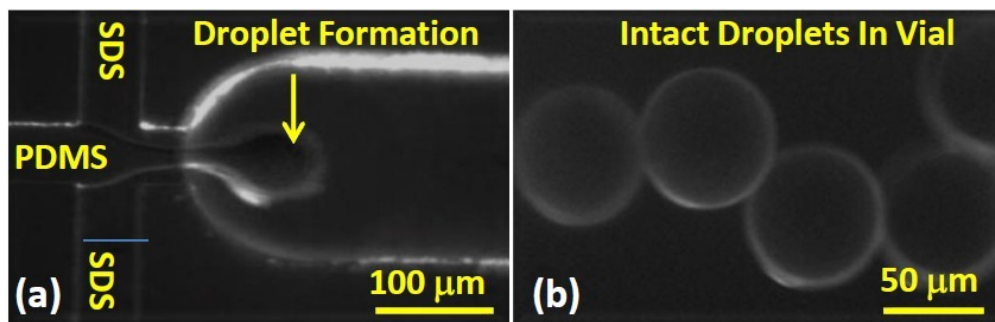


**Figure 4.2.** (a) Formation of PDMS-bearing droplets by flow focusing. The PDMS precursor stream is the central flow through the channel, while the side streams are both aqueous solutions of 5 wt% SDS. (b) Uncured PDMS droplets remain stable in a glass vial without coalescence or aggregation.

The above PDMS dispersed phase was used in our flow-focusing setup along with a continuous phase composed of the anionic surfactant SDS (5 wt%) in deionized (DI)

water. The microfluidic channels were made of PMMA treated with UV/Ozone, which ensured that the channel walls were hydrophilic (contact angle of water on such a treated PMMA surface was about  $50^\circ$ ).<sup>60</sup> Figure 4.2a shows a close-up of the entrance to the main channel from the orifice. The PDMS flow emerges through the center while the SDS solutions flow in from the side channels (top and bottom in the photo). The figure shows a droplet of PDMS being formed in the main channel and it subsequently splits off and travels down the channel. Successive droplets were similarly formed, and these were collected downstream in a glass vial. Figure 4.2b shows that the droplets remained stable (no aggregation or coalescence) in the vial, which is presumably because the surfactant SDS adsorbs on the droplets and provides electrostatic and steric stabilization. After a desired number of droplets accumulated, the vial was transferred to an oven at  $70^\circ\text{C}$  where the droplets were thermally cured into solid microbeads. Following curing, these microbeads could either be stored in the same SDS solution or centrifuged, rinsed and dried under vacuum to a powder. The dried beads could be re-dispersed in appropriate media.

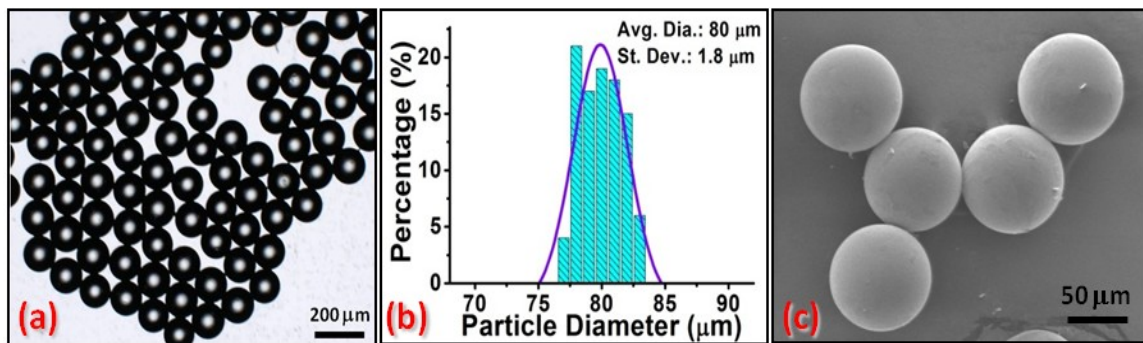


**Figure 4.3.** Images of cured PDMS microbeads from: (a) optical microscopy; and (c) SEM. In (b) the size distribution of microbeads in (a) is plotted. The average diameter of the beads is  $80\ \mu\text{m}$  with a standard deviation of  $1.8\ \mu\text{m}$ . A Gaussian fit to the distribution is also shown. Data was obtained with a sample size of 100 microbeads.

Figure 4.3 shows optical and electron micrographs of the cured PDMS microbeads. The beads are near-monodisperse and their size distribution from Figure 4.3a is plotted as a histogram in Figure 4.3b. From the data, the average diameter ( $D$ ) is determined to be  $80\ \mu\text{m}$  and the standard deviation ( $\sigma$ ) is  $1.8\ \mu\text{m}$ . The coefficient of variance ( $CV = \sigma/D \times 100$ ) is thus calculated to be 2.25%. To our knowledge, such uniformity in size has not been reported previously for PDMS microcolloids in the literature.<sup>65-67</sup> Indeed, uniformity in properties such as size is a highly desirable feature for many applications. It should be noted that the average size can be readily varied (from  $\sim 10$  to  $200\ \mu\text{m}$ ) by either altering the flow rates in our setup or by using microchannels of different diameters.

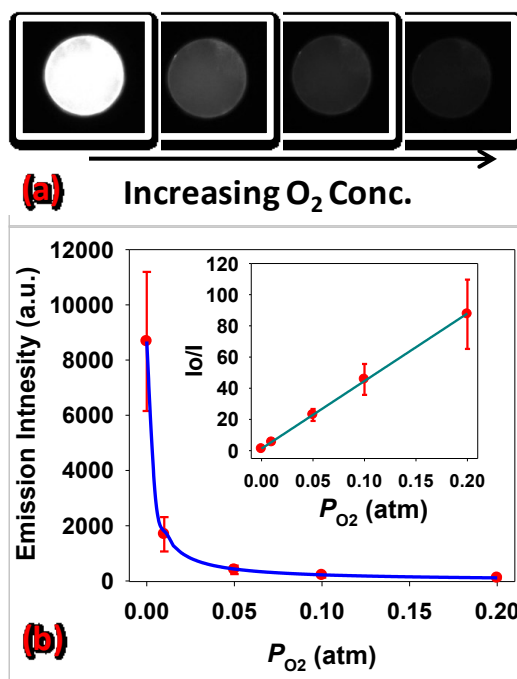


**Figure 4.4.** (a) Optical microscope images showing contrast in phosphorescence intensity of a PtTFPP-bearing PDMS microbead ( $150\ \mu\text{m}$  diameter) at various oxygen levels. (b) Plot of phosphorescence intensity vs. oxygen partial pressure. The phosphorescence is significantly quenched with increasing oxygen levels, and the response follows the Stern-Volmer equation (eq 4.1), as shown by the inset plot. Data points indicate the mean values from eight beads with standard deviations given by the vertical error bars.

### 4.3.2. Performance as Oxygen Sensors

In addition to size, the functional properties of the PDMS microbeads can also be easily varied by including appropriate payloads along with the PDMS precursor solution. As a demonstration of this capability, we incorporated an oxygen-sensitive porphyrin dye, Pt(II)-meso-tetrakis(pentafluorophenyl)-porphine (PtTFPP) into the bead matrix for the purpose of using the beads as microsensors for oxygen.<sup>74-75</sup> The principle behind oxygen (O<sub>2</sub>) sensing is that PtTFPP phosphorescence is dynamically quenched in the presence of O<sub>2</sub>.<sup>74-75</sup> Also, the high gas permeability of PDMS (800 Barrer) allows rapid permeation of O<sub>2</sub> molecules into the bead and thus ensures rapid response and high sensitivity.<sup>74</sup> The microscale size of the sensors is attractive because it allows each bead to monitor the local concentration of O<sub>2</sub> within a given volume.

Characterization of the oxygen-sensing PDMS microbeads was performed by placing the microbeads in a multiwell plate that allowed continuous flow of gas containing mixtures of pure nitrogen (0% O<sub>2</sub>) and air (21% O<sub>2</sub>) (Figure 4.1d). The beads were observed with an inverted fluorescence microscope and the emission intensity was quantified under different O<sub>2</sub> levels. As depicted in Figure 4.4, the phosphorescence is attenuated with increasing O<sub>2</sub> content. The inset shows that the quenching response follows the Stern-Volmer equation:<sup>74,76</sup>

$$\frac{I_0}{I} = 1 + K_{SV} \cdot P_{O_2} \quad (\text{eq 4.1})$$

where  $I$  is the emission intensity,  $I_0$  is the intensity in the absence of oxygen,  $K_{SV}$  is the Stern-Volmer constant, and  $P_{O_2}$  is the partial pressure of oxygen. From the slope of the

line fit,  $K_{SV}$  is calculated to be  $435 \pm 109 \text{ atm}^{-1}$  for these beads. Using this calibration, the beads can be used to detect the  $\text{O}_2$  levels in an unknown test environment and in real-time. Importantly, the beads can detect both gas-phase  $\text{O}_2$  as well as the concentration of dissolved  $\text{O}_2$  in liquids.<sup>74</sup> Such real-time monitoring of dissolved  $\text{O}_2$  in aqueous media is of great value during 3-dimensional (3-D) cell culture: for example, the growth and virulence of cancer cells is very different under hypoxic vs. ambient oxygen conditions.<sup>77-</sup>  
<sup>78</sup> Besides, in our previous studies on the PtTFPP-thin-film sensors,<sup>74</sup> no significant photobleaching effects were observed even during continuous illumination for  $>3600 \text{ s}$ , and here we anticipate similar behaviors of negligible photobleaching for these microparticulate sensors. Moreover, gradients in oxygen levels are expected to be established across a 3-D culture or a growing tumor, and the use of sensing beads will allow these local differences in oxygen levels to be probed. For such cases, it may also be advantageous to embed magnetic particles in the PDMS beads, thus allowing an individual bead to be moved by an external magnetic field to various distinct locations for oxygen sensing.<sup>79-80</sup> The beads can also be made softer or more elastic by combining the PDMS precursors with an inert, nonvolatile organic liquid prior to thermal curing.

#### **4.4. CONCLUSIONS**

In summary, we have presented a new approach to producing monodisperse PDMS microbeads through a microfluidic method. The method involves flow-focusing droplets of nonpolar PDMS-precursor (tailored to have a low viscosity) in an aqueous continuous phase bearing surfactant. The droplets are then cured off-chip to produce monodisperse beads that can be stored either as an aqueous dispersion or as a dry powder.

In addition, we have shown how specific functionalities, such as the ability to sense oxygen, can be readily imparted to the PDMS microbeads. These beads may be attractive as a substitute for traditional microparticles such as silica or latex due to their mechanical and optical properties, high gas permeability, chemical inertness, nontoxicity, and biocompatibility.

## Chapter 5

# MICROFLUIDIC SYNTHESIS OF MACROPOROUS POLYMER IMMUNOBEADS\*

### 5.1. INTRODUCTION

Macroporous polymers, whose internal structures can be tailored to exhibit pores with dimensions ranging from hundreds of nanometers to several micrometers, are widely used as stationary phases in chromatography and solid supports in affinity extraction.<sup>81-88</sup> Macroporous polymers offer outstanding mass transfer efficiency, low hydrodynamic resistance, and simple and versatile surface modifications.<sup>81-87,89-90</sup> Macroporous polymer supports are widely available in various geometries, including disks, columns, tubes, and membranes.<sup>82</sup> Facile integration of these materials into miniaturized analysis systems may also be readily achieved by taking advantage of selective *in situ* photopolymerization of the materials within optically transparent capillaries or microfluidic channels.<sup>91</sup> Furthermore, the immobilization of bioaffinity ligands, such as proteins, on their porous surfaces can enable macroporous polymers with to selectively enrich targeted biomolecules through stable and specific interactions,<sup>83-85,87,92-93</sup> allowing these materials to serve as efficient stationary supports for a range of bioaffinity chromatography and biosensing platforms such as flow-through immunosensors.<sup>92,93</sup>

---

\* The results presented in this chapter have been published in the following journal article: Jiang K.Q., Sposito A., Liu J., Raghavan S.R., DeVoe D.L. Microfluidic synthesis of macroporous polymer immunobeads. *Polymer* **2012**, **53**, 5469-5475.

Here we extend the concept of macroporous polymer-enabled biosensing to a new format consisting of functionalized macroporous methacrylate microspheres with excellent size uniformity. The microspheres are synthesized using a microfluidic co-flow emulsion technique to achieve large populations with exceptionally low polydispersity. Compared to established macroporous polymer formats, the tunable microspheres are suitable for use across a host of analytical applications or platforms, such as free-floating microbead sensors suspended in bulk solutions and multiplexed arrays of discrete sensor elements integrated within planar microfluidic devices. Here the microspheres are explored as discrete antibody-functionalized microscale immunosensor elements, or immunobeads. Solid non-porous immunobeads are routinely employed for a variety of analytical applications in the biological and medical sciences. Magnetic immunobeads have long been used in cell separation processes,<sup>94-95</sup> and multiplexed immunobead assays employing readout techniques such as optical detection,<sup>96</sup> flow cytometry,<sup>97</sup> or agglutination<sup>98</sup> have been widely commercialized.<sup>99-102</sup> The macroporous immunobeads presented here represent an attractive alternative to traditional immunobeads which typically consist of solid silica or polymer particles. Compared to these established immunobeads, the macroporous microspheres offer significantly enhanced surface/volume ratios, using a facile fabrication process yielding nearly monodisperse populations of particles that offer access to simple immobilization methods for anchoring biomolecules on their surfaces.

Continuous-flow microfluidic fabrication of macroporous polymer microbeads is described, and preparation of the full immunobeads is demonstrated by selectively

immobilizing anti-IgG antibodies on the surface of synthesized macroporous microspheres, followed by direct immunoassay characterization using fluorescein-labeled IgG as a target analyte. An efficient covalent anchoring method is described to significantly reduce background fluorescence and ensure high detection sensitivity. The resulting immunobeads reveal detection limits in the picomolar concentration range. The advantages of the macroporous structures are demonstrated through direct comparison to control samples of solid non-porous microbeads, revealing nearly order-of-magnitude improvement in detection limits for the macroporous immunobeads.

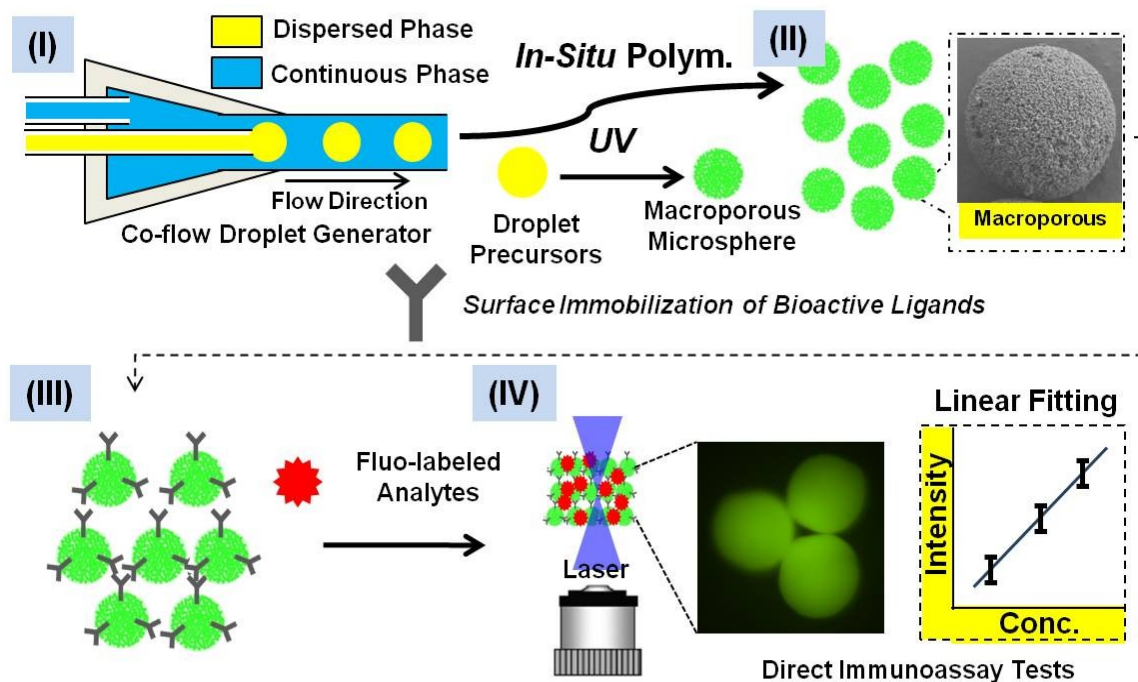


**Figure 5.1.** Schematic of the macroporous microsphere synthesis and surface modification process: (I) Microfluidic generation of droplet precursors in a co-flow droplet generator, with the dispersed phase composed of monomer GMA, crosslinker SR454, porogen DA, and photoinitiator DMPA sheared into discrete droplets by a continuous phase comprising an aqueous solution with surfactants. (II) UV photopolymerization of the droplet precursors for the formation of stable macroporous microspheres; (III) Immobilization of capture antibody on the pore surfaces converts the microspheres into active immunobeads. (IV) Direct immunoassay test of immunobeads using fluorescent labeled antigen.

## 5.2. EXPERIMENTAL SECTION

**Materials and Chemicals:** Glycidyl methacrylate (GMA), 2,2-dimethoxy-2-phenylacetophenone (DMPA), decyl alcohol (DA), polyvinyl alcohol (PVA, 30K MW), Triton X-100, ethylenediamine (EDA), N-gamma-maleimido-butyryloxy-succinimide (GMBS), bovine serum albumin (BSA), phosphate buffer (PBS), and fluorescein isothiocyanate (FITC)-labeled rabbit IgG (MW ~140 kDa) were purchased from Sigma-Aldrich. Goat anti-Rabbit IgG ((H+L) secondary antibody), methanol, acetone, and toluene were obtained from Thermo Fisher Scientific. The ethoxylated-trimethylolpropane-triacrylate (SR454) tri-vinyl acrylate crosslinker was received as a free sample from Sartomer.

**Microfluidic Device Assembly:** The microfluidic co-flow tubing device used in all experiments (Figure 5.1) was assembled from glass capillaries and microbore PTFE tubing in a manner similar to previous designs.<sup>22,103</sup> The inner glass capillary (VitroCom) was selected with dimensions of 50  $\mu\text{m}$  ID and 80  $\mu\text{m}$  OD, and the outer translucent PTFE tubing (Cole-Parmer) was chosen with an ID of 100  $\mu\text{m}$ . The inner glass capillary, cleaved at a length of 5 cm, was first connected to one end of a 2.5 cm length of 250  $\mu\text{m}$  ID and 750  $\mu\text{m}$  OD Tygon tubing (Cole-Parmer). The other end of the Tygon tubing was inserted into a 10  $\mu\text{L}$  plastic pipette tip with the end cut off. The open capillary end was positioned within the modified pipette top with a ~2 cm length outside the tip head. After inserting another Tygon tubing segment into the tail of the pipette for convenient introduction of the continuous phase, the tail was sealed with epoxy. At the pipette tip,

the glass capillary was inserted into the PTFE tubing, and the tip of the pipette was sealed with Dow Corning 3140 silicone adhesive.

**Microparticle Preparation:** For the preparation of macroporous microspheres, the dispersed phase (36 wt% GMA, 24 wt% SR454, 39 wt% DA, 1 wt% DMPA) and the continuous phase (3 wt% PVA and 1% wt Triton X-100 in water) were injected separately by two syringe pumps (PHD 2000, Harvard Apparatus). Solid non-porous microspheres for control comparison were produced in the absence of the DA porogen, using a dispersed phase mixture consisting of 59 wt% GMA, 39.4 wt% SR454, and 1.6 wt% DMPA under the same setting-up conditions for macroporous microspheres preparation. Droplets were UV-cured *in-situ* while travelling along the tubing with a total UV exposure dose of 18 mW/cm<sup>2</sup>. The stabilized microspheres were collected in a glass vial and exposed to an additional 15 min UV step at the same dose for full polymerization. After curing, the microspheres were thoroughly rinsed with methanol, acetone, toluene, acetone and DI water in sequence, and re-dispersed into 1× PBS buffer for storage. Imaging of pore morphology was performed by freezing collections of microspheres in liquid nitrogen, and cleavage the beads by a scalpel to expose the interior pores. Image analysis was performed using ImageJ software(<http://rsbweb.nih.gov/ij>).

**Surface Functionalization:** The microsphere surfaces were functionalized with bioactive proteins (anti-IgG) through two separate processing routes, namely glutaraldehyde and GMBS immobilization. In the glutaraldehyde route, the microspheres were immersed in a dilute solution of EDA in DI water (80% v/v) at 50 °C for 2 h, followed by rinsing with

DI water and suspension in 10 wt% aqueous glutaraldehyde in 1× PBS buffer at room temperature (RT) for 3 h. In the GMBS route, the microspheres were immersed into 2.5 M CYS solution at RT for 2 h, followed by thorough rinsing with 20% v/v methanol in DI water and re-suspension in 2 mM GMBS in ethanol for 2 h at RT following our previous protocol for continuous monolith functionalization.<sup>92</sup> After surface activation, the microspheres were fully washed by 1× PBS buffer and subsequently treated with goat anti-rabbit IgG antibody diluted in 1× PBS to a concentration of 50 µg/mL overnight at 4 °C. Immediately prior to testing, the microspheres were washed again with a solution of 2 mg/mL BSA in 1× PBS to block un-reacted surface sites and reduce unwanted non-specific binding.

**Immunoassay Test:** FITC-labeled rabbit IgG solutions with concentrations ascending from 2 ng/mL to 20 µg/mL were prepared in a buffer solution containing 2 mg/mL BSA in 1× PBS. The microspheres were incubated with 0.1 mL antigen solution in a glass vial for 30 min, followed by a final PBS rinse and in-solution optical detection. Fluorescent measurements for immunoassay tests were performed on a Nikon TE-2000S inverted epifluorescence microscope. An excitation wavelength within the range of 465–495 nm was selected using a B-2E/C blue filter to detect the monolith-bound antigens. Scanning electron microscopy was performed on an Hitachi SU-70 SEM to characterize the macroporous structure of the microspheres, following ~20 nm gold sputter coating for improved surface contrast.

## 5.3. RESULTS AND DISCUSSION

### 5.3.1. Macroporous Microsphere Synthesis

Microfluidic synthesis of droplets has proven to be a highly effective method for the production of microparticles with unprecedented control over size, shape, and functional properties. While a range of microfluidic-based droplet preparation methods have been reported,<sup>22</sup> all of these techniques involve the emulsification of one flow (dispersed phase) into a second immiscible flow (continuous phase) to create a stream of monodisperse droplets. For the production of solid polymer particles using this approach, the dispersed phase may consist of reactive monomers or oligomers, and these liquid droplet precursors can be subsequently be converted into solid microparticles by inducing physical or chemical crosslinking.<sup>14</sup> The size of the produced microparticles may be systematically adjusted in the range of a few micrometers to hundreds of micrometers by selecting appropriate microchannel dimensions and droplet formation topologies, fluid viscosities, and continuous/dispersed phase flow rate ratios.<sup>14,22</sup> Recently, the construction of microfluidic devices from glass capillary and plastic tubing has been used for droplet production as a simpler and more accessible alternative to traditional planar chip fabrication methods.<sup>22</sup> In the present work, a microfluidic tubing device comprising a co-flow droplet generator integrated with a downstream region for *in situ* UV polymerization was employed. A schematic of the system is shown in Figure 5.1.

The co-flow droplet generator consists of two separate capillaries assembled inside a modified pipette tip, where the outer diameter of the inner capillary was slightly smaller than the inner diameter of the outside capillary, allowing the inner capillary to fit

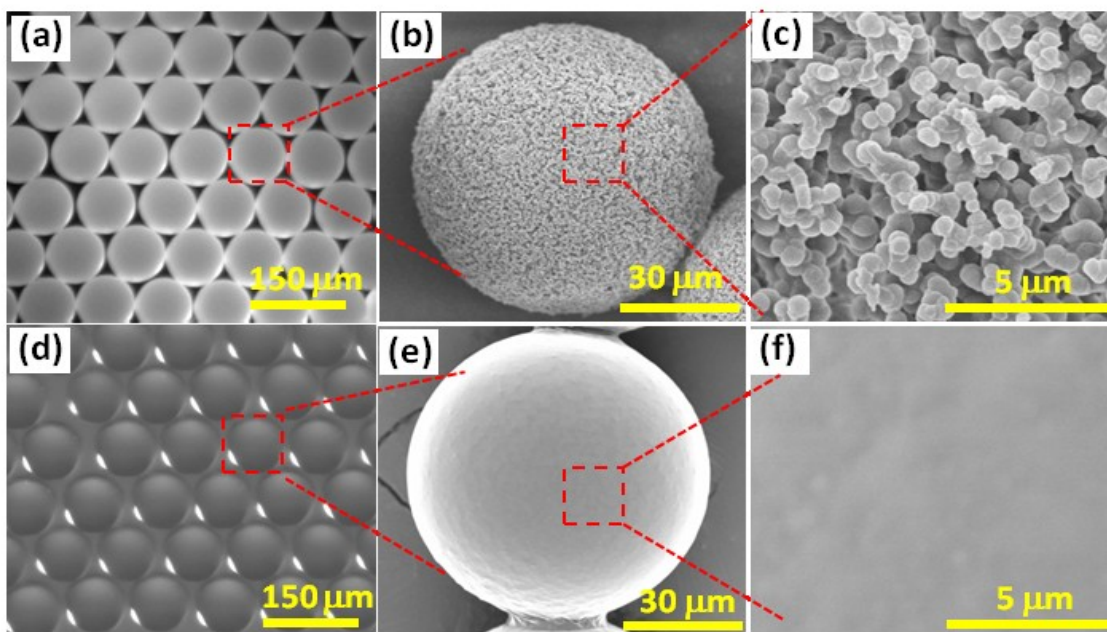


**Figure 5.2.** (a) Optical micrograph of monodisperse macroporous microspheres prepared from the precursor recipe with monomer GMA, crosslinker SR454 and porogen DA. (b) Electron micrograph of a single microbead revealing its macroporous structure. (c) Magnified view of the porous morphology. (d) Optical microscope image of solid non-porous microbeads without the addition of porogen DA during preparation. (e) Electron micrograph of a non-porous microbead. (f) Magnified view of a solid bead surface revealing the lack of macroporosity.

into the microbore of the outer capillary with a defined circumferential gap to form a simple co-flow microfluidic device. The oil-based dispersed phase, comprised of a precursor mixture of monomer, crosslinker, porogen and photoinitiator, was injected through the inner capillary in the same direction of the aqueous continuous phase flowing through the outer capillary. A surface-active polymer (PVA) and surfactant (Triton X-100) were also added in the continuous phase for improved stability during droplet generation. At the tip of the inner capillary where the two immiscible flows meet, uniform droplets formed as a result of the interfacial tension and the shearing force imposed by the continuous phase.<sup>104</sup> The droplet volume can be tuned over a range of

approximately 70-100  $\mu\text{m}$  by adjusting the relative flow rates of each fluid stream, with the upper limit dictated by the inner diameter of the sheath flow capillary. In the present work we prepared microspheres with a mean diameter of 77  $\mu\text{m}$  formed at dispersed and continuous flow rates of 2  $\mu\text{l}/\text{min}$  and 30  $\mu\text{l}/\text{min}$ , respectively. Size uniformity of the polymer microsphere under these conditions was excellent, with a standard deviation of 2.0  $\mu\text{m}$  (2.6% relative standard deviation) measured by optical characterization over a sample size of 100 microspheres.

Following droplet generation, a downstream UV-curing zone was used to convert the fluid droplets into polymerized microspheres using a long transparent tube positioned beneath a UV light source. Upon UV exposure, the droplet precursor was converted into stable solidified microparticles as the *in situ* polymerization process proceeded. This process was monitored directly by observing the change in appearance of droplets from clear to semi-opaque. The opacity arises due to the formation of porous matrix resulting from dynamic phase separation of the acrylate polymer in the presence of the DA porogen. While the monomers are soluble in DA, the polymer is not.<sup>81</sup> In the process, the polymer phase-separates into sub-micrometer particles that aggregate to form a solid, connected network within the volume with the interstices filled with DA. A typical UV exposure time of 30 seconds, defined by the total flow rate and tubing length, was found to be sufficient to partially polymerize the droplets and stabilize their shape. The resulting microspheres were collected in a glass vial pre-filled with the continuous phase solution (Figure 5.1). To ensure full conversion of the monomers, an additional 15 min UV exposure was performed following off-chip collection. Subsequently, the DA porogen

and remaining un-reacted reagents were washed from the microparticles by sequential rinses in methanol, acetone, and toluene.

In addition, non-porous microparticles were also prepared using the same procedure and experimental system, except that no porogen was added into the monomer mixture. These non-porous microparticles were used as control samples to evaluate signal enhancement for the macroporous immunobeads. No significant size variation between macroporous microspheres (77  $\mu\text{m}$ ) and non-porous microparticles (75  $\mu\text{m}$ ) was observed under the same preparation conditions for each case.

Figure 5.2a and 5.2d show optical micrographs of the macroporous and non-porous microspheres produced using this technique. In each image, populations of both microbeads present well-arranged close-packed hexagonal patterns, confirming the nearly monodisperse nature of the resulting microspheres. Electron microscopy reveals that the microspheres prepared in the presence of porogen exhibit the expected co-continuous, macroporous texture, with fused clusters of sub-micrometer polymeric globules (Figures 5.2b and 5.2c) and inter-connected flow through-pores that enable high permeability. In contrast, the solid microspheres formed in the absence of porogen do not exhibit any macroporosity. Just as with continuous monolithic stationary phase materials used in chromatography, the macroporosity of these microspheres, as well as the relative ratio of the skeletal structure and through pores, can be adjusted by varying synthesis parameters such as the relative concentrations of the monomer, crosslinker, and porogen.<sup>105-107</sup> The formation of a non-porous layer at the outer surface of the microspheres can be avoided by appropriate selection and proportion of porogens and surfactants.<sup>108</sup>

Uniform porosity was also observed throughout the entire volume of the macroporous microspheres, as revealed by SEM imaging of a cleaved microparticle in Figure 5.3a. The mean diameter of the macroporous microspheres was essentially identical to that of the non-porous control particles (Figure 5.3b), indicating that phase separation between the polymer and porogen does not result in significant loss of porogen to the surrounding continuous phase for the conditions used in this work.

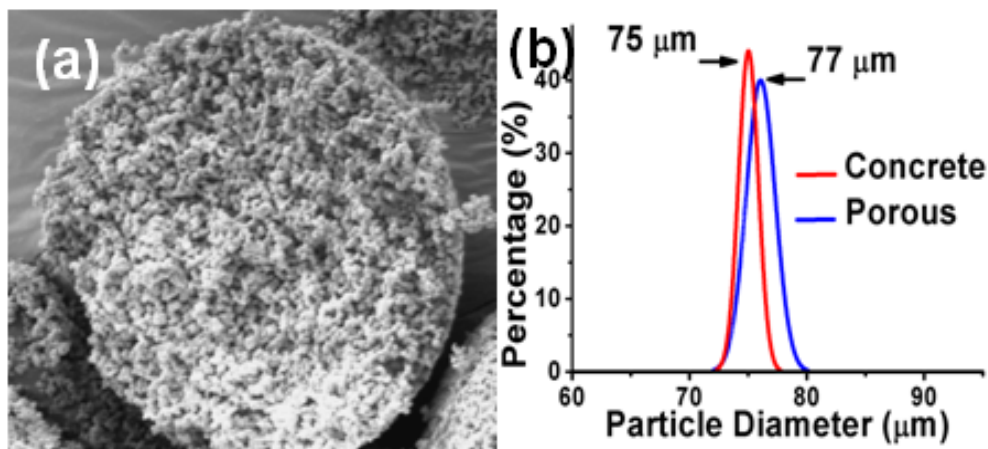


**Figure 5.3.** (a) SEM image of a cleaved macroporous microspheres revealing uniform porosity throughout the particle volume. (b) Size distributions of both macroporous microspheres and solid non-porous microparticles showing excellent size uniformity. Data was obtained with a sample size of 100 microbeads in each case.

The morphological properties of the macroporous beads were determined by image analysis of high resolution SEMs taken from cleaved microspheres. The bead matrix was observed to be formed of individual GMA particles with a mean diameter of 600 nm, arranged in random clusters ranging from linear chains of individual particles to larger fused groups with total volumes corresponding to up to approximately 12 particles. Pore dimensions were assessed by measuring the largest circle circumscribed by the surrounding polymer within a given plane of the beads, yielding a measured value of 1.6

$\pm 0.6 \mu\text{m}$ . Overall porosity was found to range between 44-50%, with no significant variation through the bead radius for any of the parameters.

The synthesis of various porous microparticles has previously been investigated using droplet microfluidics,<sup>109-114</sup> with porous structures most commonly formed from heterogeneous double emulsions that serve as templates to form voids and cavities within the final polymer spheres. In this approach, the dispersed phase is first emulsified with smaller inverted inert microemulsions that do not participate in the polymerization process. After droplet formation and polymerization, internal voids are formed by aggressive washing or evaporation to remove these inert microemulsions. The voids generated by these double emulsion methods are typically isolated, not interconnected as a result of their closed-cell morphologies, and would not benefit much for rapid molecular diffusion and transportation. In contrast, the structure of the macroporous microparticles synthesized through phase separation consists of extensively interconnected pores exhibiting an open-cell morphology. For analytical applications, this feature offers multiple pathways for rapid transport of analytes with low hydrodynamic resistance for efficient convection, and short diffusive length scales for rapid analyte/surface interactions.

Macroporous microspheres synthesized by phase separation have previously been demonstrated in work by Kumacheva et al,<sup>106</sup> in which the relationship between monomer composition and particle morphology was investigated. Here we describe a modified approach to the microfluidic synthesis of macroporous methacrylate

microspheres that offers several advantages over prior methods, and further demonstrate an effective path to surface modification of the resulting porous microspheres to anchor bioactive species, enabling their use as discrete immunosensors. A unique feature of our synthesis route is the use of trivinyl crosslinking of SR454 to achieve large pore dimensions and enhance efficient convective transport of probe and analyte molecules through the monolith matrix.<sup>92-93</sup> Moreover, we note that unlike the previous use of phthalate plasticizers as porogens,<sup>106</sup> which have recently raised wide environmental concern,<sup>115</sup> here we have adopted decyl alcohol as a much safer alcohol-based solvent as the porogen while still achieving excellent control over the resulting pore dimensions. An additional unique aspect of the platform used for macroporous microsphere synthesis is its simplicity. All components are commercially available and readily assembled without any need for complicated or costly microfabrication equipment as commonly required in conventional microfluidic droplet synthesis methods.<sup>22,64,116</sup> The tubing method provides a simple route to the production of microfluidic devices supporting co-flow droplet generation that is accessible to labs and researchers without advanced microfabrication facilities or experience, with the use of a fluoropolymer as the outer tubing material making the platform suitable for either oil-in-water or water-in-oil emulsion systems.<sup>117</sup>

### **5.3.2 Immunobead Functionalization**

A number of established routes are available to append desired surface functionalities on the macroporous polymer substrates, such as copolymerization of functional monomers, grafting functional side chains from surface reactive sites, or chemical modification of reactive functional groups. In the latter approach, various types

of bioactive ligands, including proteins, enzymes, and carbohydrates have been covalently immobilized onto macroporous polymer substrates for use as stationary phase materials in affinity chromatography.<sup>84,87</sup> Here we adopt a similar strategy for

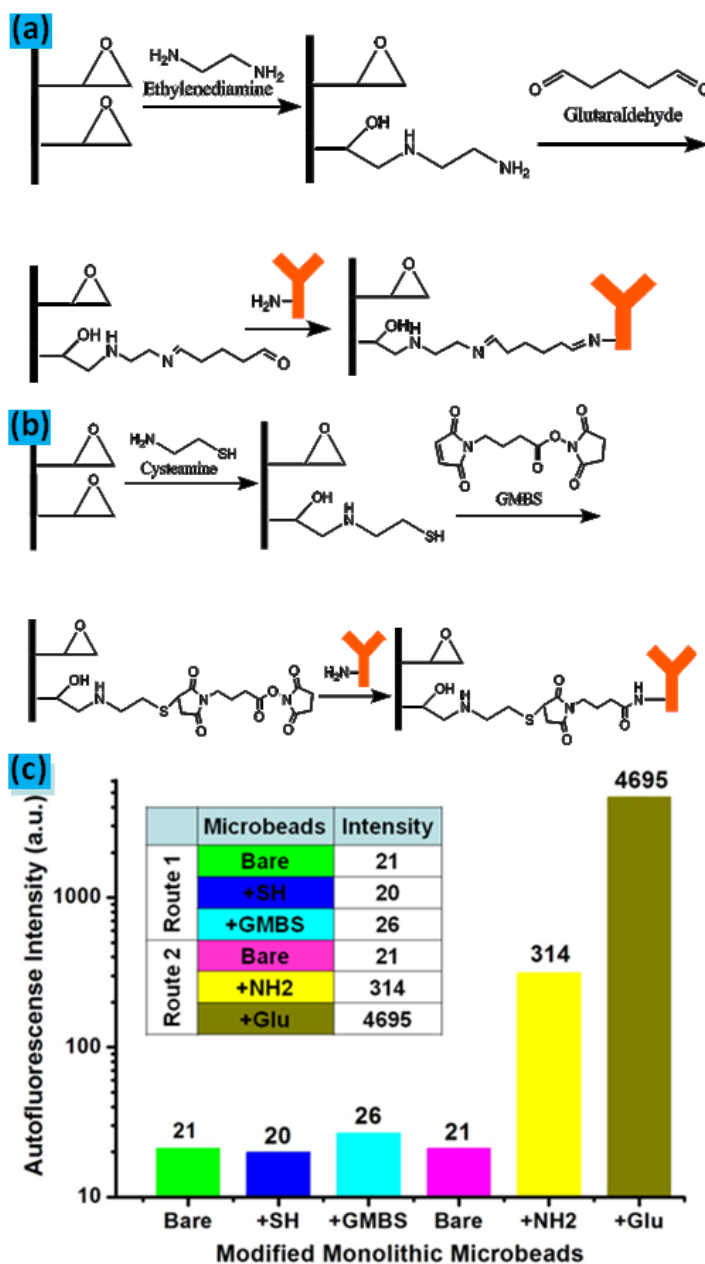


**Figure 5.4.** (a)&(b) Schematic illustrations of the GMBS and glutaraldehyde routes for immobilization of antibody on the monolith surface. (c) Auto-fluorescence measurements after each modification step reveals that the GMBS route reduces background fluorescence compared to the glutaraldehyde route by over 2 logs.

immunobead production, with the use of GMA as the macroporous polymer offering several routes to simple and facile surface functionalization.<sup>83-84,87</sup> The pendant epoxide group of the polyGMA repeat unit can be easily reacted with primary amine/thiol groups of suitable crosslinkers and biomolecules through a specific nucleophilic epoxy ring-opening reaction.<sup>87</sup> Using this approach, the content of accessible epoxide groups on the macroporous matrix can be roughly estimated by comparing the ratio of GMA/SR454 added during preparation (60:40 by weight in the present work), and should be stoichiometrically excessive for subsequent surface modification steps. Svec and co-workers studied the heterogeneous polymerization of GMA suspensions in aqueous continuous phase at the same 60 wt% feed amount and found that the GMA fraction in the polymerized product is in the range of 45% to 60%.<sup>88</sup> In addition, a variety of linking methods for epoxide-presenting surfaces are readily available, such as direct epoxy anchoring,<sup>118</sup> Schiff base reaction,<sup>83</sup> and glutaraldehyde crosslinking.<sup>84,119</sup>

As an initial study, we used glutaraldehyde, a dialdehyde crosslinker, to covalently immobilize goat anti-rabbit IgG on the surface of GMA macroporous microspheres. The GMA surface epoxides were first reacted with EDA, and then treated with glutaraldehyde through a robust aldehyde-amine reaction (Figure 5.4a). One of the two aldehyde groups in a glutaraldehyde molecule first reacted with the amine group of EDA on the macroporous polymer surface, leaving the remaining aldehyde group on the other end of the glutaraldehyde free and active. The remaining free aldehyde was then reacted with the IgG primary amines to immobilize the antibodies on the polymer surface.<sup>84</sup> Since applications of functionalized macroporous materials have mainly been

limited as monolithic stationary phases in separations or solid phases for extraction applications,<sup>82,86</sup> evaluation of their optical performance, such as the background fluorescence induced during probe grafting, has generally been neglected in previous studies. However, in order to support analytical platforms where fluorescent optical readout is desirable, the impact of background fluorescence becomes an important consideration when selecting the appropriate grafting method. The glutaraldehyde anchoring method was found to suffer from significant enhancement in background fluorescence, with a 20 times increase following the initial ethylenediamine treatment, and a 300 times increase after glutaraldehyde modification. This behavior, which has been previously observed when fixing tissue specimens with glutaraldehyde,<sup>120</sup> severely degrades the achievable fluorescence detection limits for immunobeads functionalized using this method. Another disadvantage of the glutaraldehyde route is that unsaturated imines formed during amine-aldehyde binding are susceptible to later hydrolysis under aqueous environments, thus requiring an additional stabilization step such as cyanoborohydride treatment.<sup>84</sup>

As an alternative, we explored the use of GMBS as a heterobifunctional protein crosslinker to achieve efficient surface immobilization of antibodies on the porous GMA monolith surface. In this procedure, a thiol group is first introduced to the monolith through reaction between the epoxide group and cysteamine, followed by grafting of a GMBS molecule to the newly-formed thiol through reaction with the GMBS maleimido terminus,<sup>92</sup> as depicted in Figure 5.4a. The succinimidyl ester on the other side of GMBS is then used to bind directly with the primary amine of a target protein, namely goat anti-

rabbit IgG antibody in the current study. We note that thiol groups exposed during the cysteamine reaction can themselves react with surface epoxides, thereby reducing the efficiency of GMBS anchoring on the thiol-presenting GMA surface, and alternative reaction routes capable of avoiding this path would be desirable to enhance GMBS density. Unlike the case of glutaraldehyde crosslinking, no increase in background fluorescence was observed when applying the GMBS anchoring route for antibody immobilization on the macroporous microspheres (Figure 5.4b). Moreover, the hetero-bifunctional GMBS crosslinker does not self-couple to large reactive biopolymers such as proteins and peptides, an issue with the homo-bifunctional glutaraldehyde route which could deactivate their biological functionalities. Similarly, the two termini of the glutaraldehyde molecule can react with two epoxide groups on the polymer surface, decreasing the density of available sites for protein immobilization.<sup>92</sup>

### **5.3.3. Immunobead Performance**

To evaluate the performance of the GMA-based macroporous microspheres functionalized with GMBS-immobilized antibodies, a direct immunoassay test was performed using anti-IgG as a capture ligand for fluorescently-labeled rabbit IgG as a target antigen. Because unreacted thiols remaining on the GMA surface following antibody attachment present sites for non-specific proteins interactions through exposed cysteine residues, the fabricated immunobeads were incubated with BSA as a blocking agent before use to minimize non-specific binding. The use of BSA as a blocker was chosen since this approach is routinely used in ELISA and Western blot assays for clinical diagnosis and immunology studies. During the immunoassay test, anti-IgG

functionalized macroporous microspheres were immersed into solutions of FITC-labeled IgG at concentrations ranging from 2 ng/mL to 200  $\mu$ g/mL and incubated at room temperature for 30 min. After incubation, the microspheres were rinsed thoroughly in DI water to remove possible unbound antibodies. The resulting fluorescence intensity as a function of antibody concentration is shown in Figure 5.5. The results reveal a nearly linear relation between emitted intensity and antibody concentration over a 5 log range, with a detection limit of approximately  $\sim$ 2 ng/mL ( $\sim$ 14 pM) defined by a minimum signal-to-noise ratio of S/N = 3.

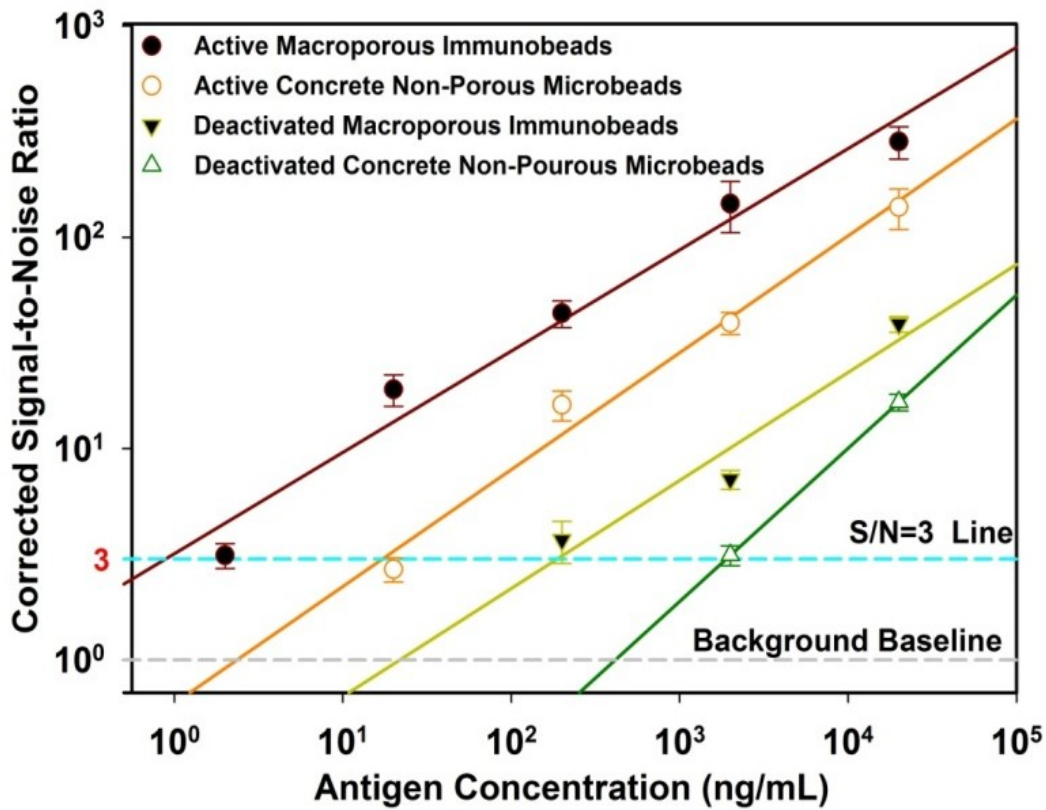


**Figure 5.5.** Performance of anti-IgG functionalized immunobeads at different FITC-IgG concentrations. Control samples with deactivated anti-IgG on both macroporous microspheres and non-porous microbeads were also prepared to assess differences between specific and non-specific binding. Error bars reflect the standard deviation of fluorescence measurements performed from 10 individual immunobeads.

To investigate the impact of microsphere macroporosity on antigen capture, a control set of non-porous microbeads was prepared from a prepolymer solution lacking the addition of porogen (Figure 5.2d-5.2f). The non-porous microbeads were functionalized with anti-IgG using the same conditions employed for the macroporous microspheres. As depicted in Figure 5.5, the fluorescence intensity of the solid, non-porous microspheres is significantly lower than the macroporous microspheres at each antibody concentration, with increasing disparity between the results at lower concentration levels. The significant difference on immunoassay performance between the two samples is attributed to the co-continuous, macroporous texture, which not only provides additional accessible surface area for the immobilization to achieve higher density of antibodies on the microsphere surface, but also encourages more efficient antibody-antigen interactions by a combination of steric entrapment and shortened diffusion lengths within the macroporous matrix.

Quantitative comparison of specific and non-specific interactions was also performed through a parallel IgG dilution study. Identical surface modification and antibody immobilization procedures were used to functionalize both macroporous and non-porous microbeads, after which the antibodies on the polymer surfaces were deactivated by additional exposure to 70 °C for 1 hr. Exposure to evaluated temperature denatures the  $F_{ab}$  fragments,<sup>121</sup> resulting in irreversible aggregation of adjacent surface-bound antibodies and disrupting their biological functionality. Both the active and deactivated immunobeads retain the similar surface properties, but with different levels of bioactivity for specific antigen-antibody binding. Compared to active immunobeads, the

deactivated microsphere exhibit a 1-2 log decrease in antibody capture for both the porous and non-porous cases, demonstrating that the majority of the fluorescence signal for the functional microparticles is due to specific interactions with surface-bound antigens as desired.

In the experiments presented here, diffusion serves as the dominant mechanism for transport of analyte through the porous beads during incubation with antigen in a static vial. For applications involving the use of fabricated microspheres in flow-through immunosensors, we note that the macroporous structure can provide a further benefit by allowing pressure-driven perfusion through the porous matrix for more rapid and efficient analyte/surface interactions. This phenomenon was recently investigated for the case of porous agarose bead sensors with sub-micrometer pore dimensions,<sup>122</sup> and was previously explored for the case of dual-porosity beads for chromatographic applications.<sup>123-124</sup> For laminar Poiseuille flow through a tube, fluid flow velocity scales with the square of the tube diameter, and thus the perfusion velocity through the immunobead pores ( $u_p$ ) relative to the interstitial flow ( $u_o$ ) can be modelled as  $u_p = (d_p^2/d_o^2)u_o$ , where  $d_p$  and  $d_o$  are the hydraulic diameters of the pores and interstitial voids between immunobeads, respectively. For the case of close-packed immunobeads, the hydraulic diameter may be approximated as the diameter of the largest sphere that can fit through the narrowest opening between the immunobeads. From geometric analysis for the 77  $\mu\text{m}$  diameter close-packed beads, the interstitial hydraulic diameter is estimated to be 12  $\mu\text{m}$ , whereas the average hydraulic diameter of the pores is 1.6  $\mu\text{m}$ . Thus the velocity of flow through the bead pores is expected to be approximately 1% of the

interstitial flow velocity. While perfusion represents only a small portion of the overall flow, the use of high total flow rates can generate significant convective transport through the beads at a higher rate than diffusion alone.

#### **5.4. Conclusions**

A discrete immunosensor technology based on macroporous polymer immunobeads formed by a phase separation process has been developed. The microspheres were synthesized from precursor mixtures using a robust, continuous-flow, and high-throughput capillary co-flow platform with excellent control over size uniformity. Multiple routes for crosslinking antibodies to the porous polymer surface were evaluated toward their impact on optical properties of the functionalized microbeads, with GMBS crosslinking identified as an efficient method yielding low autofluorescence.

Bioactive proteins were successfully anchored on the surface of the monolithic particles, enabling their use as versatile immunobeads suitable for a wide range of biosensing and bioassay applications. The combination of facile microfluidic synthesis, low polydispersity, excellent macroporosity with uniform and repeatable pore morphology, and straightforward route to biofunctionalization yielding low autofluorescence offers unique advantages toward the use of the immunobeads as discrete miniaturized biosensor elements, affinity supports for solid-phase extraction, catalyst carriers, and other applications where high surface area can enhance interactions between analytes in solution and microsphere-anchored biomolecules. The immunobeads were successfully evaluated through a direct immunoassay experiment using fluorescent

readout, revealing a linear response over 5 logs of antigen concentration and a detection limit in the ng/mL range. While this work has focused on static immersion of the sensor elements in antigen solution, the macroporous immunobeads can provide further benefits in flow-through immunosensor applications, where interstitial perfusion through the porous matrix results in rapid convective transport coupled with short diffusion length scales for improved transport of analyte molecules to the polymer surface.

## Chapter 6

# CONCLUSIONS AND RECOMMENDATIONS

### 6.1. Project Summary and Principal Contributions

In this dissertation, we have shown that the technique of droplet microfluidics provides a simple and versatile solution for the production of functional polymer microparticles. Three types of microparticles with distinct materials (i.e. chitosan microparticles, PDMS microbeads and macroporous microparticles) have been generated by delicate engineering of microfluidic devices, precursor solutions and solidification methods. Besides, we have explored the potential of these microparticles to be applied to a number of practical situations including the construction of microstructures, real-time monitoring of oxygen concentrations, and direct immunosensing of biomolecules.

**Table 6.1.** Brief summary of polymeric functional microparticles developed in this thesis.

Project	Device	Type	Polym.	Functionalization	Application
Chitosan Microparticles	PMMA <i>T Junction</i>	W/O	Chemical crosslinkage <i>"in situ"</i>	Direct Encapsulation	Micro-Assembly
PDMS Microbeads	PMMA <i>Flow Focusing</i>	O/W	Thermal Curing <i>"off chip"</i>	Direct Encapsulation	Oxygen Sensor
Macroporous Microparticles	Tubing Assembly <i>Co-Flow</i>	O/W	UV Polym. <i>"in situ"</i> + <i>"off chip"</i>	Surface Modification	Immunoassays

In chapter 3, we have confirmed that chitosan microparticles can be used as building blocks and the microchannels can be used as spatial templates for the purpose of *in situ* “bottom up” assembly. The expertise gained in this study is valuable as it lays the foundation for the construction of other additional types of microstructures, such as microsized T-shape, Y-shape, and polyhedral clusters. In addition, the engineering on the functional properties of these assembled microstructures (i.e. magnetic and fluorescent) are of critical importance before achieving the production of these proposed artificial microswimmers.

In classical techniques, the emulsification of PDMS precursors into uniform droplets is generally problematic due to their inherent high viscosity and low surface energy. In Chapter 4 we have demonstrated a viable approach to solve these problems. The high shear force provided by microfluidics ensures the successful shearing of PDMS mixtures into discrete droplets, and the addition of appropriate surfactants effectively prevents these droplets from unwanted coalescence. Although the presented work focuses on the case of PDMS materials, the resulting microfluidic design is applicable for the dispersion of other viscous mixtures like hydrogels.

In Chapter 5 we describe a successful interdisciplinary effort to translate a traditional macroporous stationary phase into a new type of discrete microparticle immunosensors. The unique synthesis and functionalization path offers significant contributions toward a diverse range of biological and chemical sensing applications. We have also noticed the problem of background fluorescence during surface

functionalization, which has generally been neglected in previous studies. The GMBS modification approach developed here that offers minimum auto-fluorescence would be of interest to scientists who want to optimize the detection limit of their optical immunosensors. In addition, the simplicity of the tubing device fabrication provides easy access to droplet microfluidic techniques without the need of advanced fabrication facilities.

## **6.2. RECOMMENDATIONS FOR FUTURE WORK**

Based on the microfluidic technique we have reported, it is highly possible to explore new possibilities following the platform and expertise we have developed. Here we briefly describe the work for the future as below:

### **6.2.1. Chitosan Microparticle Assembly**

In chapter 3 we describe a microfluidic approach for the generation of microsized chitosan microparticles and their controlled assembly into complex, high-ordered micro chains. In the future we will continue on this subject to improve the performance of such magnetic microchains, while at the same time we will also explore the possibility to achieve the construction of microstructures in high throughput, continuous formats.

In order to improve the performance, it is needed first to obtain a comprehensive study of the functional properties of such assembled microchains and thus further improve their functional performance. We hope that our research on this project could contribute to the study of biomimics (like fabrication of artificial microswimmers).

Furthermore, magnetic responsiveness and chain flexibility of these microchains are of critical importance. The two key properties are further affected by a variety of additional parameters, including the amount of encapsulated magnetic nanoparticles, the size and shape of the microparticle subunits, as well as the stiffness of the intraparticle interaction. These parameters need to be studied first before achieving the production of such proposed artificial microswimmers.

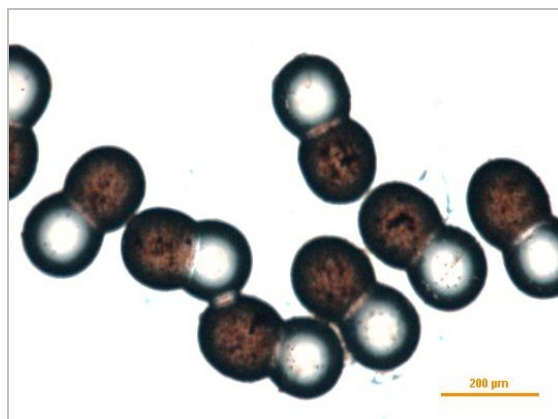


**Figure 6.1.** Bi-functional dimers assembled from chitosan microparticles, each lobe of the dimmer can have distinctive properties. The assembly process is achieved *in-situ* by a highly controlled microfluidic-mediated coalescence behavior that pairs two individual droplets together.

Second, we would like to improve the throughput of the assembly route by improving our platform design. In Chapter 3 the throughput of our chain assembly is constrained by the manual operation to block channel outlet, and thus is not sustainable for scale up production. As part of future work, we will explore the possibility of developing automatic, continuous assembly platforms that could produce microparticles as in assemblies “streamline” assemblies of manufacturing factories. This could be obtained by the integration of additional components into the microfluidic chip. For example, we are interested in adding a droplet coalescence chamber in our platform that

could align two distinctive droplets in pair and link them together though highly regulated manner, so that we can produce structures of dimers automatically.

### **6.2.2. PDMS Microparticles: Synthesis and Other Applications**

Our plan for future work of PDMS microparticles will focus on a more comprehensive and systematic study on them. Additional efforts will be devoted to optimize their functional properties of such microbeads (including particle size, stiffness), as well as to expand their applications into broader areas. Specific goals in this part of the project include:

First we would like to scale down the size of microbeads toward additional applications. Currently the typical size of generated PDMS microbeads is in the range of 50  $\mu\text{m}$  to 200  $\mu\text{m}$ . Although such a size range is sufficient for many applications, some may require PDMS microparticles with smaller diameters. For example, if we can engineer these microbeads to sub-micrometer scale, they may be able to circulate within blood vessels and provide real-time monitoring of oxygen concentration in human body. This size decrease can be achieved by using microfluidic channels with smaller sizes or by other alternative methods.

In addition, we also want to optimize the properties of PDMS microbeads and improve their functional performance. We would like to make microbeads of varying mechanical properties. For example, we can vary the weight ratio of the PDMS precursor and curing agent, or dilute the PDMS mixture by additional solvents (i.e. nonvolatile

silicone oils). Thereby, we can obtain the range from stiff beads to soft, compliant beads. Soft beads that are swollen with solvent could possibly encapsulate greater amounts of dye. Also, the diffusion of oxygen or other analytes could be varied in the case of softer beads.

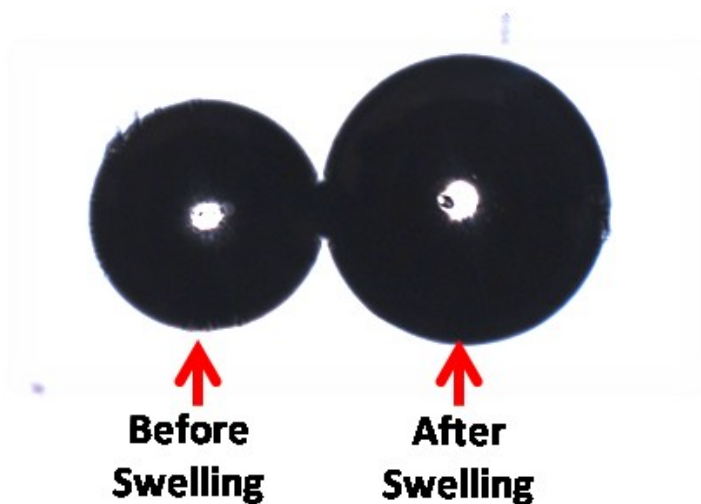


**Figure 6.2.** The significant swelling of PDMS microparticle in the oil-based limonene compound demonstrates their excellent loading capacity for hydrophobic encapsulants. It allows these PDMS microparticles to be used as controlled release carriers which can carry a load of encapsulants and then slowly release them.

Moreover, we wish to expand these PDMS microbeads into wider application fields. These PDMS microbeads have already been demonstrated as excellent oxygen sensing microparticles, however, their potential is not just limited by this application. They possess many advantageous properties, including elasticity, transparency, low size distribution and biological/chemical stability. We believe that these novel microparticles can be used as alternatives to substitute traditional micro-particles (silica/polylatex microbeads) in many circumstances.

### **6.2.3. Macroporous Microparticles: Other Applications**

In Chapter 5 we have demonstrated the success of these macroporous microparticles as high performance immunosensors by functionalizing their surface with antigen/antibody. In the future we are expecting to functionalize these microparticles with other types of chemical/bio specific agents, such as biotin/streptavidin, DNA, gold nanoparticles and many others, so that we can expand to enable their usage in a diverse range of applications such as separation, sensing, proteomics and genomics.

## REFERENCES

- [1] Nussinovitch, A. *Polymer macro- and micro-gel beads : fundamentals and applications*; Springer: New York, 2010.
- [2] Kawaguchi, H. "Functional polymer microspheres." *Progress in Polymer Science* **2000**, 25, 1171-1210.
- [3] Levinson, R.; Royal Society of Chemistry (Great Britain) *More modern chemical techniques*; Royal Society of Chemistry: London, 2001.
- [4] Merkel, T. J.; Herlihy, K. P.; Nunes, J.; Orgel, R. M.; Rolland, J. P.; DeSimone, J. M. "Scalable, Shape-Specific, Top-Down Fabrication Methods for the Synthesis of Engineered Colloidal Particles." *Langmuir* **2010**, 26, 13086-13096.
- [5] Häfeli, U. *Scientific and clinical applications of magnetic carriers*; Plenum Press: New York, 1997.
- [6] Ogura, Y.; Kimura, H. "Biodegradable polymer microspheres for targeted drug delivery to the retinal pigment epithelium." *Surv Ophthalmol* **1995**, 39 Suppl 1, S17-24.
- [7] Rosen, M. R. *Delivery system handbook for personal care and cosmetic products : technology, applications, and formulations*; William Andrew Pub.: Norwich, NY, 2005.
- [8] Sakka, S. *Handbook of sol-gel science and technology : processing, characterization, and applications*; Kluwer Academic Publishers: Boston, 2005.
- [9] Fang, A. P.; Cathala, B. "Smart swelling biopolymer microparticles by a microfluidic approach Synthesis, in situ encapsulation and controlled release." *Colloids and Surfaces B-Biointerfaces* **2011**, 82, 81-86.
- [10] Champion, J. A.; Katare, Y. K.; Mitragotri, S. "Particle shape: A new design parameter for micro- and nanoscale drug delivery carriers." *Journal of Controlled Release* **2007**, 121, 3-9.
- [11] Yoo, J. W.; Irvine, D. J.; Discher, D. E.; Mitragotri, S. "Bio-inspired, bioengineered and biomimetic drug delivery carriers." *Nature Reviews Drug Discovery* **2011**, 10, 521-535.
- [12] Pichot, C. "Recent Developments in the Functionalization of Latex-Particles." *Makromolekulare Chemie-Macromolecular Symposia* **1990**, 35-6, 327-347.
- [13] Urban, D.; Takamura, K. *Polymer dispersions and their industrial applications*; Wiley-VCH: Weinheim, 2002.

- [14] Il Park, J.; Saffari, A.; Kumar, S.; Gunther, A.; Kumacheva, E. "Microfluidic Synthesis of Polymer and Inorganic Particulate Materials." *Annual Review of Materials Research, Vol 40* **2010**, *40*, 415-443.
- [15] Teh, S. Y.; Lin, R.; Hung, L. H.; Lee, A. P. "Droplet microfluidics." *Lab on a Chip* **2008**, *8*, 198-220.
- [16] Christopher, G. F.; Anna, S. L. "Microfluidic methods for generating continuous droplet streams." *Journal of Physics D-Applied Physics* **2007**, *40*, R319-R336.
- [17] Solvas, X. C. I.; deMello, A. "Droplet microfluidics: recent developments and future applications." *Chemical Communications* **2011**, *47*, 1936-1942.
- [18] Abate, A. R.; Krummel, A. T.; Lee, D.; Marquez, M.; Holtze, C.; Weitz, D. A. "Photoreactive coating for high-contrast spatial patterning of microfluidic device wettability." *Lab on a Chip* **2008**, *8*, 2157-2160.
- [19] Zheng, B.; Tice, J. D.; Ismagilov, R. F. "Formation of droplets of in microfluidic channels alternating composition and applications to indexing of concentrations in droplet-based assays." *Analytical Chemistry* **2004**, *76*, 4977-4982.
- [20] Seemann, R.; Brinkmann, M.; Pfohl, T.; Herminghaus, S. "Droplet based microfluidics." *Reports on Progress in Physics* **2012**, *75*.
- [21] Umbanhowar, P. B.; Prasad, V.; Weitz, D. A. "Monodisperse emulsion generation via drop break off in a coflowing stream." *Langmuir* **2000**, *16*, 347-351.
- [22] Shah, R. K.; Shum, H. C.; Rowat, A. C.; Lee, D.; Agresti, J. J.; Utada, A. S.; Chu, L. Y.; Kim, J. W.; Fernandez-Nieves, A.; Martinez, C. J.; Weitz, D. A. "Designer emulsions using microfluidics." *Materials Today* **2008**, *11*, 18-27.
- [23] Nie, Z. H.; Seo, M. S.; Xu, S. Q.; Lewis, P. C.; Mok, M.; Kumacheva, E.; Whitesides, G. M.; Garstecki, P.; Stone, H. A. "Emulsification in a microfluidic flow-focusing device: effect of the viscosities of the liquids." *Microfluidics and Nanofluidics* **2008**, *5*, 585-594.
- [24] Xu, J. H.; Li, S. W.; Tan, J.; Wang, Y. J.; Luo, G. S. "Controllable preparation of monodisperse O/W and W/O emulsions in the same microfluidic device." *Langmuir* **2006**, *22*, 7943-7946.
- [25] Gross, G. A.; Hamann, C.; Gunther, M.; Kohler, J. M. "Formation of polymer and nanoparticle doped polymer minirods by use of the microsegmented flow principle." *Chemical Engineering & Technology* **2007**, *30*, 341-346.

- [26] Cho, S. H.; Jun, J. B.; Ryu, J. H.; Suh, K. D. "Preparation of monodisperse poly (divinylbenzene) macrobeads via a drop breaking and polymerization method." *Colloids and Surfaces a-Physicochemical and Engineering Aspects* **2005**, *254*, 1-7.
- [27] Nisisako, T.; Torii, T.; Higuchi, T. "Novel microreactors for functional polymer beads." *Chemical Engineering Journal* **2004**, *101*, 23-29.
- [28] Jiang, K. Q.; Thomas, P. C.; Forry, S. P.; DeVoe, D. L.; Raghavan, S. R. "Microfluidic synthesis of monodisperse PDMS microbeads as discrete oxygen sensors." *Soft Matter* **2012**, *8*, 923-926.
- [29] Iwamoto, S.; Nakagawa, K.; Sugiura, S.; Nakajima, M. "Preparation of gelatin microbeads with a narrow size distribution using microchannel emulsification." *AAPS PharmSciTech* **2002**, *3*, E25.
- [30] Tadmouri, R.; Romano, M.; Guillemot, L.; Mondain-Monval, O.; Wunenburger, R.; Leng, J. "Millifluidic production of metallic microparticles." *Soft Matter* **2012**, *8*, 10704-10711.
- [31] Helgeson, M. E.; Chapin, S. C.; Doyle, P. S. "Hydrogel microparticles from lithographic processes: Novel materials for fundamental and applied colloid science." *Current Opinion in Colloid & Interface Science* **2011**, *16*, 106-117.
- [32] Tumarkin, E.; Kumacheva, E. "Microfluidic generation of microgels from synthetic and natural polymers." *Chemical Society Reviews* **2009**, *38*, 2161-2168.
- [33] Jiang, K. Q.; Xue, C.; Arya, C. D.; Shao, C. R.; George, E. O.; DeVoe, D. L.; Raghavan, S. R. "A New Approach to In-Situ "Micromanufacturing": Microfluidic Fabrication of Magnetic and Fluorescent Chains Using Chitosan Microparticles as Building Blocks." *Small* **2011**, *7*, 2470-2476.
- [34] Zhang, H.; Tumarkin, E.; Peerani, R.; Nie, Z.; Sullan, R. M. A.; Walker, G. C.; Kumacheva, E. "Microfluidic production of biopolymer microcapsules with controlled morphology." *Journal of the American Chemical Society* **2006**, *128*, 12205-12210.
- [35] Qin, D.; Xia, Y. N.; Whitesides, G. M. "Soft lithography for micro- and nanoscale patterning." *Nature Protocols* **2010**, *5*, 491-502.
- [36] Tsao, C. W.; DeVoe, D. L. "Bonding of thermoplastic polymer microfluidics." *Microfluidics and Nanofluidics* **2009**, *6*, 1-16.
- [37] Castro-Hernandez, E.; Gundabala, V.; Fernandez-Nieves, A.; Gordillo, J. M. "Scaling the drop size in coflow experiments." *New Journal of Physics* **2009**, *11*.

- [38] Furst, E. M.; Suzuki, C.; Fermigier, M.; Gast, A. P. "Permanently linked monodisperse paramagnetic chains." *Langmuir* **1998**, *14*, 7334-7336.
- [39] Biswal, S. L.; Gast, A. P. "Mechanics of semiflexible chains formed by poly(ethylene glycol)-linked paramagnetic particles." *Physical Review E* **2003**, *68*, -.
- [40] Biswal, S. L.; Gast, A. P. "Rotational dynamics of semiflexible paramagnetic particle chains." *Physical Review E* **2004**, *69*, -.
- [41] Biswal, S. L.; Gast, A. P. "Micromixing with linked chains of paramagnetic particles." *Analytical Chemistry* **2004**, *76*, 6448-6455.
- [42] Dreyfus, R.; Baudry, J.; Roper, M. L.; Fermigier, M.; Stone, H. A.; Bibette, J. "Microscopic artificial swimmers." *Nature* **2005**, *437*, 862-865.
- [43] Sacanna, S.; Irvine, W. T. M.; Chaikin, P. M.; Pine, D. J. "Lock and key colloids." *Nature* **2010**, *464*, 575-578.
- [44] Yin, Y. D.; Lu, Y.; Gates, B.; Xia, Y. N. "Template-assisted self-assembly: A practical route to complex aggregates of monodispersed colloids with well-defined sizes, shapes, and structures." *Journal of the American Chemical Society* **2001**, *123*, 8718-8729.
- [45] Yin, Y. D.; Xia, Y. N. "Self-assembly of spherical colloids into helical chains with well-controlled handedness." *Journal of the American Chemical Society* **2003**, *125*, 2048-2049.
- [46] Xia, Y. N.; Yin, Y. D.; Lu, Y.; McLellan, J. "Template-assisted self-assembly of spherical colloids into complex and controllable structures." *Advanced Functional Materials* **2003**, *13*, 907-918.
- [47] Wu, H. K.; Thalladi, V. R.; Whitesides, S.; Whitesides, G. M. "Using hierarchical self-assembly to form three-dimensional lattices of spheres." *Journal of the American Chemical Society* **2002**, *124*, 14495-14502.
- [48] Kim, S. H.; Jeon, S. J.; Yi, G. R.; Heo, C. J.; Choi, J. H.; Yang, S. M. "Optofluidic assembly of colloidal photonic crystals with controlled sizes, shapes, and structures." *Advanced Materials* **2008**, *20*, 1649-+.
- [49] Bouquey, M.; Serra, C.; Berton, N.; Prat, L.; Hadziioannou, G. "Microfluidic synthesis and assembly of reactive polymer beads to form new structured polymer materials." *Chemical Engineering Journal* **2008**, *135*, S93-S98.
- [50] Singh, H.; Laibinis, P. E.; Hatton, T. A. "Rigid, superparamagnetic chains of permanently linked beads coated with magnetic nanoparticles. Synthesis and

- rotational dynamics under applied magnetic fields." *Langmuir* **2005**, *21*, 11500-11509.
- [51] Subramaniam, A. B.; Abkarian, M.; Stone, H. A. "Controlled assembly of jammed colloidal shells on fluid droplets." *Nature Materials* **2005**, *4*, 553-556.
- [52] Sung, K. E.; Vanapalli, S. A.; Mukhija, D.; Mckay, H. A.; Millunchick, J. M.; Burns, M. A.; Solomon, M. J. "Programmable fluidic production of microparticles with configurable anisotropy." *Journal of the American Chemical Society* **2008**, *130*, 1335-1340.
- [53] Vanapalli, S. A.; Iacovella, C. R.; Sung, K. E.; Mukhija, D.; Millunchick, J. M.; Burns, M. A.; Glotzer, S. C.; Solomon, M. J. "Fluidic assembly and packing of microspheres in confined channels." *Langmuir* **2008**, *24*, 3661-3670.
- [54] Steinbacher, J. L.; McQuade, D. T. "Polymer chemistry in flow: New polymers, beads, capsules, and fibers." *Journal of Polymer Science Part a-Polymer Chemistry* **2006**, *44*, 6505-6533.
- [55] Zhang, H.; Tumarkin, E.; Sullan, R. M. A.; Walker, G. C.; Kumacheva, E. "Exploring microfluidic routes to microgels of biological polymers." *Macromolecular Rapid Communications* **2007**, *28*, 527-538.
- [56] Jahn, A.; Reiner, J. E.; Vreeland, W. N.; DeVoe, D. L.; Locascio, L. E.; Gaitan, M. "Preparation of nanoparticles by continuous-flow microfluidics." *Journal of Nanoparticle Research* **2008**, *10*, 925-934.
- [57] Dendukuri, D.; Doyle, P. S. "The Synthesis and Assembly of Polymeric Microparticles Using Microfluidics." *Advanced Materials* **2009**, *21*, 4071-4086.
- [58] Link, D. R.; Anna, S. L.; Weitz, D. A.; Stone, H. A. "Geometrically mediated breakup of drops in microfluidic devices." *Physical Review Letters* **2004**, *92*, -.
- [59] Jameela, S. R.; Jayakrishnan, A. "Glutaraldehyde Cross-Linked Chitosan Microspheres as a Long-Acting Biodegradable Drug-Delivery Vehicle - Studies on the in-Vitro Release of Mitoxantrone and in-Vivo Degradation of Microspheres in Rat Muscle." *Biomaterials* **1995**, *16*, 769-775.
- [60] Tsao, C. W.; Hromada, L.; Liu, J.; Kumar, P.; DeVoe, D. L. "Low temperature bonding of PMMA and COC microfluidic substrates using UV/ozone surface treatment." *Lab on a Chip* **2007**, *7*, 499-505.
- [61] Chen, C. F.; Liu, J. K.; Chang, C. C.; DeVoe, D. L. "High-pressure on-chip mechanical valves for thermoplastic microfluidic devices." *Lab on a Chip* **2009**, *9*, 3511-3516.

- [62] Yang, S.; Liu, J. K.; Lee, C. S.; Devoe, D. L. "Microfluidic 2-D PAGE using multifunctional in situ polyacrylamide gels and discontinuous buffers." *Lab on a Chip* **2009**, *9*, 592-599.
- [63] Chen, C. F.; Liu, J.; Hromada, L. P.; Tsao, C. W.; Chang, C. C.; DeVoe, D. L. "High-pressure needle interface for thermoplastic microfluidics." *Lab on a Chip* **2009**, *9*, 50-55.
- [64] Xia, Y. N.; Whitesides, G. M. "Soft lithography." *Angewandte Chemie-International Edition* **1998**, *37*, 551-575.
- [65] Goller, M. I.; Obey, T. M.; Teare, D. O. H.; Vincent, B.; Wegener, M. R. "Inorganic "silicone oil" microgels." *Colloids and Surfaces a-Physicochemical and Engineering Aspects* **1997**, *123*, 183-193.
- [66] Buzio, R.; Bosca, A.; Krol, S.; Marchetto, D.; Valeri, S.; Valbusa, U. "Deformation and adhesion of elastomer poly(dimethylsiloxane) colloidal AFM probes." *Langmuir* **2007**, *23*, 9293-9302.
- [67] Dufaud, O.; Favre, E.; Sadtler, V. "Porous elastomeric beads from crosslinked emulsions." *Journal of Applied Polymer Science* **2002**, *83*, 967-971.
- [68] Crisp, A.; Dejuan, E.; Tiedeman, J. "Effect of Silicone Oil Viscosity on Emulsification." *Archives of Ophthalmology* **1987**, *105*, 546-550.
- [69] Koh, A.; Gillies, G.; Gore, J.; Saunders, B. R. "Flocculation and coalescence of oil-in-water poly(dimethylsiloxane) emulsions." *Journal of Colloid and Interface Science* **2000**, *227*, 390-397.
- [70] Seo, M.; Nie, Z. H.; Xu, S. Q.; Mok, M.; Lewis, P. C.; Graham, R.; Kumacheva, E. "Continuous microfluidic reactors for polymer particles." *Langmuir* **2005**, *21*, 11614-11622.
- [71] Abate, A. R.; Thiele, J.; Weinhart, M.; Weitz, D. A. "Patterning microfluidic device wettability using flow confinement." *Lab on a Chip* **2010**, *10*, 1774-1776.
- [72] Seo, M.; Paquet, C.; Nie, Z. H.; Xu, S. Q.; Kumacheva, E. "Microfluidic consecutive flow-focusing droplet generators." *Soft Matter* **2007**, *3*, 986-992.
- [73] Bhushan, B.; Hansford, D.; Lee, K. K. "Surface modification of silicon and polydimethylsiloxane surfaces with vapor-phase-deposited ultrathin fluorosilane films for biomedical nanodevices." *Journal of Vacuum Science & Technology A* **2006**, *24*, 1197-1202.

- [74] Thomas, P. C.; Halter, M.; Tona, A.; Raghavan, S. R.; Plant, A. L.; Forry, S. P. "A Noninvasive Thin Film Sensor for Monitoring Oxygen Tension during in Vitro Cell Culture." *Analytical Chemistry* **2009**, *81*, 9239-9246.
- [75] Lee, S. K.; Okura, I. "Photostable optical oxygen sensing material: Platinum tetrakis(pentafluorophenyl)porphyrin immobilized in polystyrene." *Analytical Communications* **1997**, *34*, 185-188.
- [76] Lakowicz, J. R. *Principles of Fluorescence Spectroscopy*; Plenum Press: New York, 1983.
- [77] Atkuri, K. R.; Herzenberg, L. A.; Niemi, A. K.; Cowan, T.; Herzenberg, L. A. "Importance of culturing primary lymphocytes at physiological oxygen levels." *Proceedings of the National Academy of Sciences of the United States of America* **2007**, *104*, 4547-4552.
- [78] Brown, J. M.; Williams, W. R. "Exploiting tumour hypoxia in cancer treatment." *Nature Reviews Cancer* **2004**, *4*, 437-447.
- [79] Peng, S. L.; Zhang, M. Y.; Niu, X. Z.; Wen, W. J.; Sheng, P.; Liu, Z. Y.; Shi, J. "Magnetically responsive elastic microspheres." *Applied Physics Letters* **2008**, *92*, -.
- [80] Jiang, K.; Xue, C.; Arya, C.; Shao, C.; George, E. O.; DeVoe, D. L.; Raghavan, S. R. "A New Approach to In-Situ "Micromanufacturing": Microfluidic Fabrication of Magnetic and Fluorescent Chains Using Chitosan Microparticles as Building Blocks." *Small* **2011**, DOI: 10.1002/sml.201100514.
- [81] Okay, O. "Macroporous copolymer networks." *Progress in Polymer Science* **2000**, *25*, 711-779.
- [82] Svec, F. "Preparation and HPLC applications of rigid macroporous organic polymer monoliths." *Journal of Separation Science* **2004**, *27*, 747-766.
- [83] Jiang, T.; Mallik, R.; Hage, D. S. "Affinity monoliths for ultrafast immunoextraction." *Analytical Chemistry* **2005**, *77*, 2362-2372.
- [84] Mallik, R.; Hage, D. S. "Affinity monolith chromatography." *Journal of Separation Science* **2006**, *29*, 1686-1704.
- [85] Potter, O. G.; Hilder, E. F. "Porous polymer monoliths for extraction: Diverse applications and platforms." *Journal of Separation Science* **2008**, *31*, 1881-1906.
- [86] Svec, F. "Porous polymer monoliths: Amazingly wide variety of techniques enabling their preparation." *Journal of Chromatography A* **2010**, *1217*, 902-924.

- [87] Tetala, K. K. R.; van Beek, T. A. "Bioaffinity chromatography on monolithic supports." *Journal of Separation Science* **2010**, *33*, 422-438.
- [88] Svec, F.; Hradil, J.; Coupek, J.; Kalal, J. "Reactive Polymers .1. Macroporous Methacrylate Copolymers Containing Epoxy Groups." *Angewandte Makromolekulare Chemie* **1975**, *48*, 135-143.
- [89] Peters, E. C.; Petro, M.; Svec, F.; Frechet, J. M. J. "Molded rigid polymer monoliths as separation media for capillary electrochromatography. 1. Fine control of porous properties and surface chemistry." *Analytical Chemistry* **1998**, *70*, 2288-2295.
- [90] Vázquez, M.; Paull, B. "Review on recent and advanced applications of monoliths and related porous polymer gels in micro-fluidic devices." *Analytica Chimica Acta* **2010**, *668*, 100-113.
- [91] Nischang, I.; Brueggemann, O.; Svec, F. "Advances in the preparation of porous polymer monoliths in capillaries and microfluidic chips with focus on morphological aspects." *Analytical and Bioanalytical Chemistry* **2010**, *397*, 953-960.
- [92] Liu, J. K.; Chen, C. F.; Chang, C. W.; DeVoe, D. L. "Flow-through immunosensors using antibody-immobilized polymer monoliths." *Biosensors & Bioelectronics* **2010**, *26*, 182-188.
- [93] Liu, J. K.; White, I.; DeVoe, D. L. "Nanoparticle-Functionalized Porous Polymer Monolith Detection Elements for Surface-Enhanced Raman Scattering." *Analytical Chemistry* **2011**, *83*, 2119-2124.
- [94] Rye, P. D.; Hoifodt, H. K.; Overli, G. E.; Fodstad, O. "Immunobead filtration: a novel approach for the isolation and propagation of tumor cells." *Am J Pathol* **1997**, *150*, 99-106.
- [95] Hardingham, J. E.; Kotasek, D.; Farmer, B.; Butler, R. N.; Mi, J. X.; Sage, R. E.; Dobrovic, A. "Immunobead-Pcr - a Technique for the Detection of Circulating Tumor-Cells Using Immunomagnetic Beads and the Polymerase Chain-Reaction." *Cancer Research* **1993**, *53*, 3455-3458.
- [96] Morgan, E.; Varro, R.; Sepulveda, H.; Ember, J. A.; Apgar, J.; Wilson, J.; Lowe, L.; Chen, R.; Shivraj, L.; Agadir, A.; Campos, R.; Ernst, D.; Gaur, A. "Cytometric bead array: a multiplexed assay platform with applications in various areas of biology." *Clinical Immunology* **2004**, *110*, 252-266.
- [97] Vignali, D. A. A. "Multiplexed particle-based flow cytometric assays." *Journal of Immunological Methods* **2000**, *243*, 243-255.

- [98] Elshal, M. F.; McCoy, J. P. "Multiplex bead array assays: performance evaluation and comparison of sensitivity to ELISA." *Methods* **2006**, *38*, 317-23.
- [99] Pollema, C. H.; Ruzicka, J.; Christian, G. D.; Lernmark, A. "Sequential injection immunoassay utilizing immunomagnetic beads." *Analytical Chemistry* **1992**, *64*, 1356-1361.
- [100] Evans, M. L.; Chan, P. J.; Patton, W. C.; King, A. "A convenient mixed immunobeads screen for antisperm antibodies during routine semen analysis." *Fertil Steril* **1998**, *70*, 344-9.
- [101] Arellano-Garcia, M. E.; Hu, S.; Wang, J.; Henson, B.; Zhou, H.; Chia, D.; Wong, D. T. "Multiplexed immunobead-based assay for detection of oral cancer protein biomarkers in saliva." *Oral Dis* **2008**, *14*, 705-12.
- [102] Dekking, E. H.; van der Velden, V. H.; Varro, R.; Wai, H.; Bottcher, S.; Kneba, M.; Sonneveld, E.; Koning, A.; Boeckx, N.; Van Poecke, N.; Lucio, P.; Mendonca, A.; Sedek, L.; Szczepanski, T.; Kalina, T.; Kanderova, V.; Hoogeveen, P.; Flores-Montero, J.; Chillon, M. C.; Orfao, A.; Almeida, J.; Evans, P.; Cullen, M.; Noordijk, A. L.; Vermeulen, P. M.; de Man, M. T.; Dixon, E. P.; Comans-Bitter, W. M.; van Dongen, J. J. "Flow cytometric immunobead assay for fast and easy detection of PML-RARA fusion proteins for the diagnosis of acute promyelocytic leukemia." *Leukemia* **2012**, *26*, 1976-85.
- [103] Hwang, H.; Kim, S.-H.; Yang, S.-M. "Microfluidic fabrication of SERS-active microspheres for molecular detection." *Lab on a Chip* **2011**, *11*, 87-92.
- [104] Jeong, W. J.; Kim, J. Y.; Choo, J.; Lee, E. K.; Han, C. S.; Beebe, D. J.; Seong, G. H.; Lee, S. H. "Continuous Fabrication of Biocatalyst Immobilized Microparticles Using Photopolymerization and Immiscible Liquids in Microfluidic Systems." *Langmuir* **2005**, *21*, 3738-3741.
- [105] Wang, Q. C.; Hosoya, K.; Svec, F.; Frechet, J. M. J. "Polymeric Porogens Used in the Preparation of Novel Monodispersed Macroporous Polymeric Separation Media for High-Performance Liquid-Chromatography." *Analytical Chemistry* **1992**, *64*, 1232-1238.
- [106] Dubinsky, S.; Zhang, H.; Nie, Z. H.; Gourevich, I.; Voicu, D.; Deetz, M.; Kumacheva, E. "Microfluidic synthesis of macroporous copolymer particles." *Macromolecules* **2008**, *41*, 3555-3561.
- [107] Beiler, B.; Vincze, A.; Svec, F.; Safrany, A. "Poly(2-hydroxyethyl acrylate-co-ethyleneglycol dimethacrylate) monoliths synthesized by radiation polymerization in a mold." *Polymer* **2007**, *48*, 3033-3040.

- [108] Dubinsky, S.; Park, J. I.; Gourevich, I.; Chan, C.; Deetz, M.; Kumacheva, E. "Toward Controlling the Surface Morphology of Macroporous Copolymer Particles." *Macromolecules* **2009**, *42*, 1990-1994.
- [109] Zhang, H.; Cooper, A. I. "Synthesis and applications of emulsion-templated porous materials." *Soft Matter* **2005**, *1*, 107-113.
- [110] Partap, S.; Rehman, I.; Jones, J. R.; Darr, J. A. "“Supercritical Carbon Dioxide in Water” Emulsion-Templated Synthesis of Porous Calcium Alginate Hydrogels." *Advanced Materials* **2006**, *18*, 501-504.
- [111] Zhou, W. Q.; Gu, T. Y.; Su, Z. G.; Ma, G. H. "Synthesis of macroporous poly(styrene-divinyl benzene) microspheres by surfactant reverse micelles swelling method." *Polymer* **2007**, *48*, 1981-1988.
- [112] Zhou, W. Q.; Gu, T. Y.; Su, Z. G.; Ma, G. H. "Synthesis of macroporous poly(glycidyl methacrylate) microspheres by surfactant reverse micelles swelling method." *European Polymer Journal* **2007**, *43*, 4493-4502.
- [113] Choi, S.-W.; Zhang, Y.; Xia, Y. "Fabrication of Microbeads with a Controllable Hollow Interior and Porous Wall Using a Capillary Fluidic Device." *Advanced Functional Materials* **2009**, *19*, 2943-2949.
- [114] Fernández-Trillo, F.; van Hest, J. C. M.; Thies, J. C.; Michon, T.; Weberskirch, R.; Cameron, N. R. "Reversible Immobilization onto PEG-based Emulsion-templated Porous Polymers by Co-assembly of Stimuli Responsive Polymers." *Advanced Materials* **2009**, *21*, 55-59.
- [115] Yen, T.-H.; Lin-Tan, D.-T.; Lin, J.-L. "Food safety involving ingestion of foods and beverages prepared with phthalate-plasticizer-containing clouding agents." *Journal of the Formosan Medical Association* **2011**, *110*, 671-684.
- [116] Becker, H.; Gartner, C. "Polymer microfabrication methods for microfluidic analytical applications." *Electrophoresis* **2000**, *21*, 12-26.
- [117] Nightingale, A. M.; Krishnadasan, S. H.; Berhanu, D.; Niu, X.; Drury, C.; McIntyre, R.; Valsami-Jones, E.; deMello, J. C. "A stable droplet reactor for high temperature nanocrystal synthesis." *Lab on a Chip* **2011**, *11*, 1221-1227.
- [118] Mallik, R.; Jiang, T.; Hage, D. S. "High-Performance Affinity Monolith Chromatography: Development and Evaluation of Human Serum Albumin Columns." *Analytical Chemistry* **2004**, *76*, 7013-7022.
- [119] Petro, M.; Svec, F.; Fréchet, J. M. J. "Immobilization of trypsin onto “molded” macroporous poly(glycidyl methacrylate-co-ethylene dimethacrylate) rods and

- use of the conjugates as bioreactors and for affinity chromatography." *Biotechnology and Bioengineering* **1996**, *49*, 355-363.
- [120] Collins, J. S.; Goldsmith, T. H. "Spectral Properties of Fluorescence Induced by Glutaraldehyde Fixation." *Journal of Histochemistry & Cytochemistry* **1981**, *29*, 411-414.
- [121] Vermeer, A. W. P.; Norde, W. "The thermal stability of immunoglobulin: Unfolding and aggregation of a multi-domain protein." *Biophysical Journal* **2000**, *78*, 394-404.
- [122] Chou, J.; Lennart, A.; Wong, J.; Ali, M. F.; Floriano, P. N.; Christodoulides, N.; Camp, J.; McDevitt, J. T. "Modeling Analyte Transport and Capture in Porous Bead Sensors." *Analytical Chemistry* **2012**, *84*, 2569-2575.
- [123] Li, Q.; Zhu, J.; Daugulis, A. J.; Hsu, C. C.; Goosen, M. F. A. "Polysaccharide Microcapsules and Macroporous Beads for Enhanced Chromatographic-Separation." *Biomaterials Artificial Cells and Immobilization Biotechnology* **1993**, *21*, 391-398.
- [124] Gustavsson, P. E.; Axelsson, A.; Larsson, P. O. "Direct measurements of convective fluid velocities in superporous agarose beads." *Journal of Chromatography A* **1998**, *795*, 199-210.